Transport of fungal RAB11 secretory vesicles involves myosin-5, dynein/dynactin/p25, and kinesin-1 and is independent of kinesin-3

Miguel A. Peñalva[a,*], Jun Zhang[b], Xin Xiang[b], and Areti Pantazopoulou[a]
[a]Department of Cellular and Molecular Biology, Centro de Investigaciones Biológicas, Consejo Superior de Investigaciones Científicas, Madrid 28040, Spain; [b]Department of Biochemistry and Molecular Biology, Uniformed Services University of the Health Sciences, Bethesda, MD 20814-4799

ABSTRACT **Hyphal tip cells of the fungus *Aspergillus nidulans* are useful for studying long-range intracellular traffic. Post-Golgi secretory vesicles (SVs) containing the RAB11 orthologue RabE engage myosin-5 as well as plus end– and minus end–directed microtubule motors, providing an experimental system with which to investigate the interplay between microtubule and actin motors acting on the same cargo. By exploiting the fact that depolymerization of F-actin unleashes SVs focused at the apex by myosin-5 to microtubule-dependent motors, we establish that the minus end–directed transport of SVs requires the dynein/dynactin supercomplex. This minus end–directed transport is largely unaffected by genetic ablation of the Hook complex adapting early endosomes (EEs) to dynein but absolutely requires p25 in dynactin. Thus dynein recruitment to two different membranous cargoes, namely EEs and SVs, requires p25, highlighting the importance of the dynactin pointed-end complex to scaffold cargoes. Finally, by studying the behavior of SVs and EEs in null and rigor mutants of kinesin-3 and kinesin-1 (UncA and KinA, respectively), we demonstrate that KinA is the major kinesin mediating the anterograde transport of SVs. Therefore SVs arrive at the apex of *A. nidulans* by anterograde transport involving cooperation of kinesin-1 with myosin-5 and can move away from the apex powered by dynein.**

Monitoring Editor
Gero Steinberg
University of Exeter

Received: Aug 3, 2016
Revised: Jan 31, 2017
Accepted: Feb 7, 2017

INTRODUCTION

Intracellular transport is crucial for eukaryotic cells. Cytoplasmic dynein (Cianfrocco *et al.*, 2015) and kinesin(s) (Vale, 2003) move cargo toward the minus and plus ends of microtubules (MTs), respectively, whereas myosin-5 transports cargo toward the barbed ends of actin filaments (AFs; Reck-Peterson *et al.*, 2000; Hammer and Sellers, 2012). Within the cell, the directionality of transport is dictated by the localization and orientation of cytoskeletal tracks. For example, the orientation of MTs radiating from perinuclear MT-organizing centers (MTOCs) in higher eukaryotic cells implies that plus end–directed kinesins normally mediate centrifugal transport, whereas cytoplasmic dynein mediates centripetal transport. Certain filamentous fungi, such as *Ustilago maydis* and *Aspergillus nidulans*, are genetically amenable and experimentally advantageous to study long-distance transport due to the large intracellular distances within their tubular cells, denoted hyphae (Peñalva *et al.*, 2012; Steinberg, 2014; Xiang *et al.*, 2015). In hyphal tip cells, which grow by apical extension, centrifugal and centripetal transport correspond to anterograde (apex-directed, acropetal) and retrograde (away from the apex, basipetal) transport, respectively.

In both *U. maydis* and *A. nidulans*, early endosomes (EEs) are the best-studied dynein cargo. EEs move by kinesin-3 toward the MT plus ends at the hyphal tip and by dynein away from the hyphal tip, toward MT minus ends associated with MTOCs embedded in the nuclear membranes (Wedlich-Soldner *et al.*, 2002; Lenz *et al.*, 2006; Abenza *et al.*, 2009, 2010, 2012; Zekert and Fischer, 2009; Egan *et al.*, 2012; Seidel *et al.*, 2012, 2013). The physical interaction between dynein and EEs is mediated by the dynactin and

This article was published online ahead of print in MBoC in Press (http://www.molbiolcell.org/cgi/doi/10.1091/mbc.E16-08-0566) on February 16, 2017.

*Address correspondence to: Miguel A. Peñalva (penalva@cib.csic.es).

Abbreviations used: AF, actin filament; EE, early endosome; latB, latrunculin B; MT, microtubule; MTOC, microtubule-organizing center; SPK, Spitzenkörper; SV, secretory vesicle; TGN, *trans*-Golgi network; wt, wild type.

Supplemental Material can be found at:
http://www.molbiolcell.org/content/suppl/2017/02/12/mbc.E16-08-0566v1.DC1

Hook complexes (Zhang *et al.*, 2011b, 2014; Bielska *et al.*, 2014). Of note, several other cargoes, including mRNAs, polysomes, peroxisomes, lipid droplets, and septins, move along MTs by hitchhiking on EEs (Higuchi *et al.*, 2014; Guimaraes *et al.*, 2015; Haag *et al.*, 2015; Pohlmann *et al.*, 2015; Salogiannis *et al.*, 2016; Zander *et al.*, 2016), and for some cargoes, specific adapters linking them to EEs have been found (Pohlmann *et al.*, 2015; Salogiannis *et al.*, 2016; Salogiannis and Reck-Peterson, 2017).

Vegetative hyphae of *A. nidulans* are well suited for study of the transport of secretory vesicles (SVs) that connect the *trans*-Golgi (TGN) with the plasma membrane (PM). These SVs arise from the TGN by maturation (Pantazopoulou *et al.*, 2014; Pinar *et al.*, 2015), which involves the recruitment to TGN cisternae of *A. nidulans* RabE^{RAB11} and the subsequent engagement of the molecular motors that mediate the delivery of SVs to the apex, where they accumulate before undergoing fusion with the plasma membrane. As exocytosis supports apical extension, transport impairment slows down growth, besides altering morphology. *A. nidulans* exocytosis is an example of cooperation between actin and MT motors (Horio and Oakley, 2005; Taheri-Talesh *et al.*, 2008, 2012; Zhang *et al.*, 2011a; Pantazopoulou *et al.*, 2014). Evidence supports a relay mechanism (Figure 1A) by which SVs are moved by kinesin(s) from apex-distal regions to the hyphal tip, where they are handed over to the MyoE myosin-5 for the final step of transport to the plasma membrane (Sharpless and Harris, 2002; Taheri-Talesh *et al.*, 2012; Pantazopoulou *et al.*, 2014). It is of note that SVs are loaded with kinesin(s) and with the single *A. nidulans* myosin-5, MyoE (Pantazopoulou *et al.*, 2014). They appear to be also loaded with a minus end–directed motor, supposedly dynein. In the current model, if the relay between MTs and AFs fails, SVs move away from the tip toward the minus ends of MTs and then shift their direction to start another round of anterograde transport by kinesin(s)/myosin-5 (Figure 1A).

Cooperation between kinesin(s), myosin-5, and, hypothetically, dynein in the transport of *A. nidulans* SVs is interesting for two reasons: one is that in this cooperation, the fungus resembles higher eukaryotes (Wu *et al.*, 1998; Hammer and Sellers, 2012). The second and more important is that SVs are well suited to investigate how cargo is engaged simultaneously by different motors, which are the physiological consequences of physical interactions between kinesin and myosin-5 (Huang *et al.*, 1999), and how one motor affects the other's tracks when they coexist as passengers of the same cargo (Chesarone-Cataldo *et al.*, 2011).

Here we demonstrate that SVs can indeed engage dynein. Although EEs and SVs move independently of each other, they share the requirement for the p25 subunit of dynactin to recruit the dynein supercomplex, suggesting that p25 might play a broad role in connecting several membranous cargoes to dynactin. However, EEs and SVs differ in two important features: one is that, unlike EEs, SVs do not require the Hook complex to engage dynein. The other is that, unlike EEs, which use kinesin-3 (UncA in *A. nidulans*) for their plus end–directed movement (Wedlich-Soldner *et al.*, 2002; Zekert and Fischer, 2009; Schuster *et al.*, 2011; Egan *et al.*, 2012; Seidel *et al.*, 2013), SVs use mainly, if not exclusively, the *A. nidulans* kinesin-1, KinA.

RESULTS

In the steady state, SVs labeled with RabE^{RAB11} accumulate in the apex, forming a structure denoted Spitzenkörper (SPK; Figure 1A). Kinesin(s) and the MyoE myosin-5 cooperate to deliver SVs to the tip region (see later discussion), and yet the sharp focusing of SVs at the SPK is solely mediated by the myosin-5, exploiting the network of AFs that radiate from the apex (Sharpless and Harris, 2002;

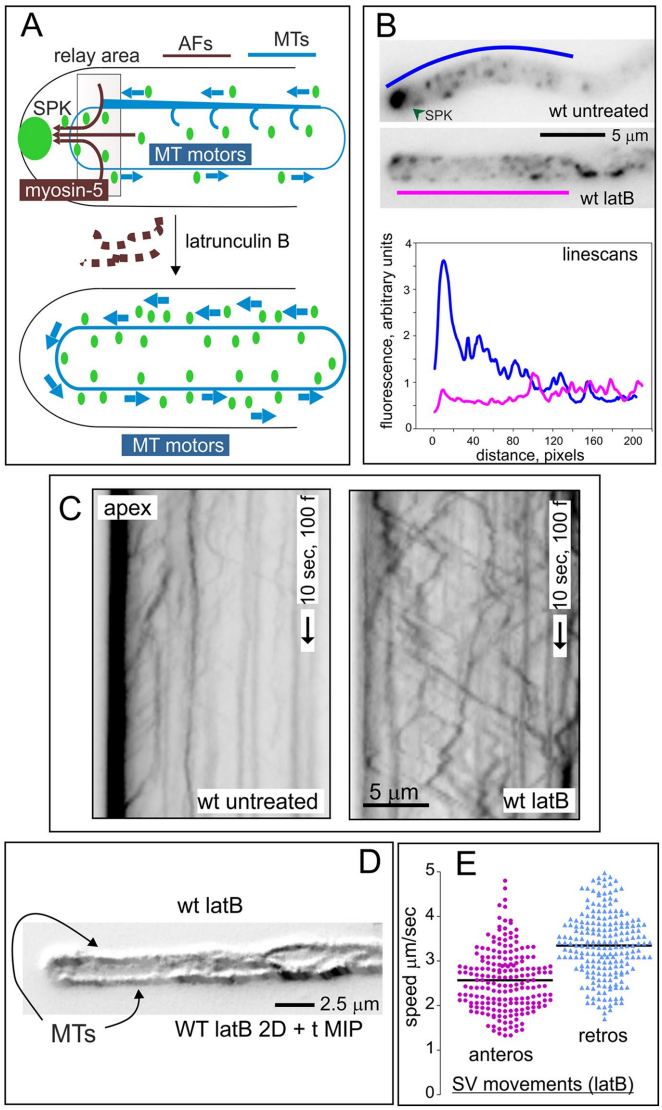

FIGURE 1: Interplay between F-actin and MT motors in the transport of *A. nidulans* SVs: the effects of depolymerizing F-actin. (A) Kinesin moves RabE^{RAB11}-containing SVs (small green ovals) to the tip region, where they are handed over to myosin-5, which normally powers the AF-dependent final stage of exocytosis between the TGN cisternae and the apex. After arriving at the SPK (an apical accumulation of SVs), a minor proportion undergoes transport away from the apex. Latrunculin B treatment releases SVs localized by actomyosin in the SPK. These unleashed SVs undertake plus end– and minus end–directed conveyor belt–like movement using MT motors. (B) Top, delocalization of the SPK GFP-RabE SVs that results from AF depolymerization. Bottom, line scans derived using the regions indicated in blue and magenta for untreated and latB-treated wt cells, respectively. (C) Kymographs derived from the same hyphae and lines used for the line scans in B. The strong signal at the apex of the untreated cell corresponds to the SPK. Time resolution, 10 frames/s. (D) Maximal intensity projection of the time stack used in C for the wt cell treated with latB. (E) Average speeds of SVs derived from kymographs for 199 anterograde and 209 retrograde SV movements pooled from three wt hyphae treated with latB at 28°C. Mean values were statistically significant ($p < 0.0001$) in an unpaired *t* test.

Taheri-Talesh *et al.*, 2012; Pantazopoulou *et al.*, 2014). Supplemental Movie S1 illustrates the strong accumulation of SVs at the apex, using moving EEs as internal reference. EEs move on dynein and

kinesin but, unlike SVs, do not engage MyoE and are uniformly distributed across hyphae.

Depolymerization of the tip network of AFs with the anti–F-actin drug latrunculin B (latB) rapidly dissipates the SPK, both by eliminating the MyoE-driven transport of SVs to the apex and by preventing the MyoE-independent tethering of SVs to AFs (Pantazopoulou *et al.*, 2014; Figure 1, A and B). The two effects combined unleash SVs to MT-dependent motors, resulting in the plus end– and minus end–directed conveyor belt–like movement of SVs that is conveniently displayed by kymographs, in which traffic shows up as diagonal tracks whose slopes correspond to the speeds of individual runs (Figure 1C). Maximal intensity projections (MIPs) of time stacks of SVs in latB-treated hyphae indeed reveal the MT tracks (Figure 1D). Supplemental Movie S2 depicts a latB-treated hypha in which the latB conveyor-like movement of SVs and the long-distance transport of EEs were cofilmed. Comparison of Supplemental Movies S1 and S2 helps in appreciating the remarkable effect that depolymerizing F-actin causes on SVs.

To determine the speed at which SVs move in this latB conveyor belt, we drew kymographs covering the apicalmost 20 µm of hyphae and tracked SVs manually, using MetaMorph software. Figure 1E shows pooled data of anterograde and retrograde runs for latB-treated hyphae cultured at 28°C. (Here and throughout the text, we use the terms anterograde and retrograde to indicate movement toward or away from the tip, respectively, rather than the direction of traffic toward or away from the plasma membrane.) Retrograde runs were, on average, significantly faster than anterograde runs (2.6 ± 0.7 SD vs. 3.3 ± 0.7 SD µm/s; $p < 0.0001$ in an unpaired *t* test). In the tip region, MTs are oriented with their plus ends toward the apex (Han *et al.*, 2001; Egan *et al.*, 2012). Therefore these data extend our previous observations indicating that SVs engage minus end–directed motors and plus end–directed kinesin(s) (Pantazopoulou *et al.*, 2014).

Retrograde transport of RabE^{RAB11} secretory vesicles: a dynein functional assay

To study the involvement of dynein in the retrograde movement of SVs, we determined with the latB conveyor belt assay the effects of heat-sensitive (*ts*) mutations affecting key components of the dynein pathway, namely the dynein heavy chain (HC) NudA (*nudA2^{ts}* and *nudA5^{ts}*), the dynein regulator NudF^{LIS1} (*nudF7*), and the dynactin constituent NudK^{ARP1} (*nudK317*; see scheme of the dynein–dynactin complex in Figure 2A). The yeast orthologue of NudF binds the HC and prevents its detachment from MTs even during cycles of ATP hydrolysis (Huang *et al.*, 2012; Toropova *et al.*, 2014). In *A. nidulans*, and *U. maydis*, NudF^{LIS1} is required for initiation of dynein-mediated endosome movement (Lenz *et al.*, 2006; Egan *et al.*, 2012). ARP1 (NudK) is the major subunit of the actin-like minifilament within the dynactin complex (Chowdhury *et al.*, 2015; Urnavicius *et al.*, 2015), and thus its mutational inactivation is expected to result in a dynactin deficit. Dynactin binds to and collaborates with cargo adaptors to increase dynein processivity (Cianfrocco *et al.*, 2015)

Strains carrying *nudA2^{ts}*, *nudA5^{ts}*, *nudF7^{ts}*, and *nudK317^{ts}* grow normally at 28°C but show characteristic *nud* mutant growth at 37°C (Supplemental Figure S1), indicating compromised function of the dynein complex. None of the mutants showed signs of disorganization or hypertrophy of the GFP-RabE^{RAB11} SPK at 28°C or after a 45- to 90-min incubation at 37°C (Supplemental Figure S1). In wild-type (wt) cells shifted to 37°C, latB also delocalized SVs to the MT conveyor belt, as at 28°C. We acquired stacks of images over time and used them to draw kymographs covering the apicalmost 20 µm of hyphae. Tracking of runs captured by kymographs in wt cells treated with latB at 37°C revealed average speeds of 3.5 ± 0.9 SD and 4.5 ± 1.1 SD µm/s for anterograde and retrograde runs, respectively (Figure 2B). This significant difference observed between anterograde and retrograde speeds ($p < 0.0001$ in unpaired *t* test) is consistent with the notion that different MT motors mediate anterograde and retrograde runs. Of note, measured average speeds at 37°C were ~35% higher than those at 28°C (Figures 1E and 2B). Next we used latB to treat *nud* mutants that had been previously shifted to 37°C for 30-45 min, seeking to impair the motor's function before unleashing SVs from the SPK. In the wt and in all four dynein pathway mutants, latB caused SV detachment from the apex. However, whereas SVs redistributed across hyphae more or less uniformly in the wt, they remained clustered in the tip regions in *nudA2*, *nudA5*, *nudF7*, and *nudK317* strains (Figure 2, C–E), indicating that their retrograde transport requires dynein. Because the *nudA2*, *nudA5*, *nudF7*, and *nudK317* alleles may differ in their severity and they affect proteins with different roles, any conclusion obtained by comparing mutant strains should be interpreted with caution. Despite this caveat, all four mutants showed a remarkably similar phenotype, presenting large aggregates of SVs within the ~5-µm most-apical region of hyphae that were absent from the wt.

We acquired stacks of images over time of latB-treated mutants (time resolution, 400 frame/min, 100–300 frames each). Movies showed that the tip aggregates were subject to forces acting in the retrograde direction and suggested that even though motors attempted to pull the mutants' aggregates away from the apex, they were incapable of dispersing them retrogradely, which is consistent with a dynein defect. A typical example is shown in Supplemental Movie S3, which is a composite showing a *nudA5* movie alongside a control movie of the wt subject to the same experimental regime. Movies also showed that very few runs were visually noticeable in the mutants, an observation that was confirmed with kymographs (Figure 2E). In stark contrast with the numerous anterograde and retrograde trajectories of SVs detached from the SPK at 37°C in the wt, only a few trajectories were detectable in the mutants (Figure 2E), and these become visible only after overcontrasting the kymographs strongly. The observation that not only retrograde movements but also anterograde ones were very scarce in latB-treated *nud* cells strongly suggests that in the wt it is the pool of RabE^{RAB11} SVs residing in the SPK (and not SVs generated de novo) that represents the major source of membranous structures moving on the latB conveyor belt. Indeed, inspection of *nud* hyphal tips immediately after addition of latB showed that the subapical clusters seen in the mutants are formed by detachment of SVs that had already accumulated at the SPK. Taken together, the foregoing data led us to conclude that the blockade at the tip region of the latB-triggered retrograde transport of SPK SVs provides an easily scorable assay for dynein function.

Recruitment of the dynein complex to SVs requires the dynactin component p25 but not the EE adaptor HookA

EEs move on MTs. EEs are loaded with dynein within the tip region (the dynein loading zone; Lenz *et al.*, 2006; Schuster *et al.*, 2011). Engagement of EEs to dynein requires dynactin, specifically its p25 subunit (Zhang *et al.*, 2011b; Figure 2A), and the Hook (FHF) complex adaptor (Bielska *et al.*, 2014; Yao *et al.*, 2014; Zhang *et al.*, 2014), which is an effector of GTPase RAB5 acting on the membrane of EEs (Guo *et al.*, 2016). Accordingly, in *p25Δ* or *hookAΔ* cells, EEs remain stalled in the tip due to their inability to move in the retrograde direction (Bielska *et al.*, 2014; Yao *et al.*, 2014; Zhang *et al.*, 2014), as shown in the RabA^{RAB5} channels of Supplemental Movies S4 and S5 and in Supplemental Figure S2. SVs gather at the SPK of *p25Δ* and *hookAΔ* hyphae as in the wt (Figure 3A and Supplemental

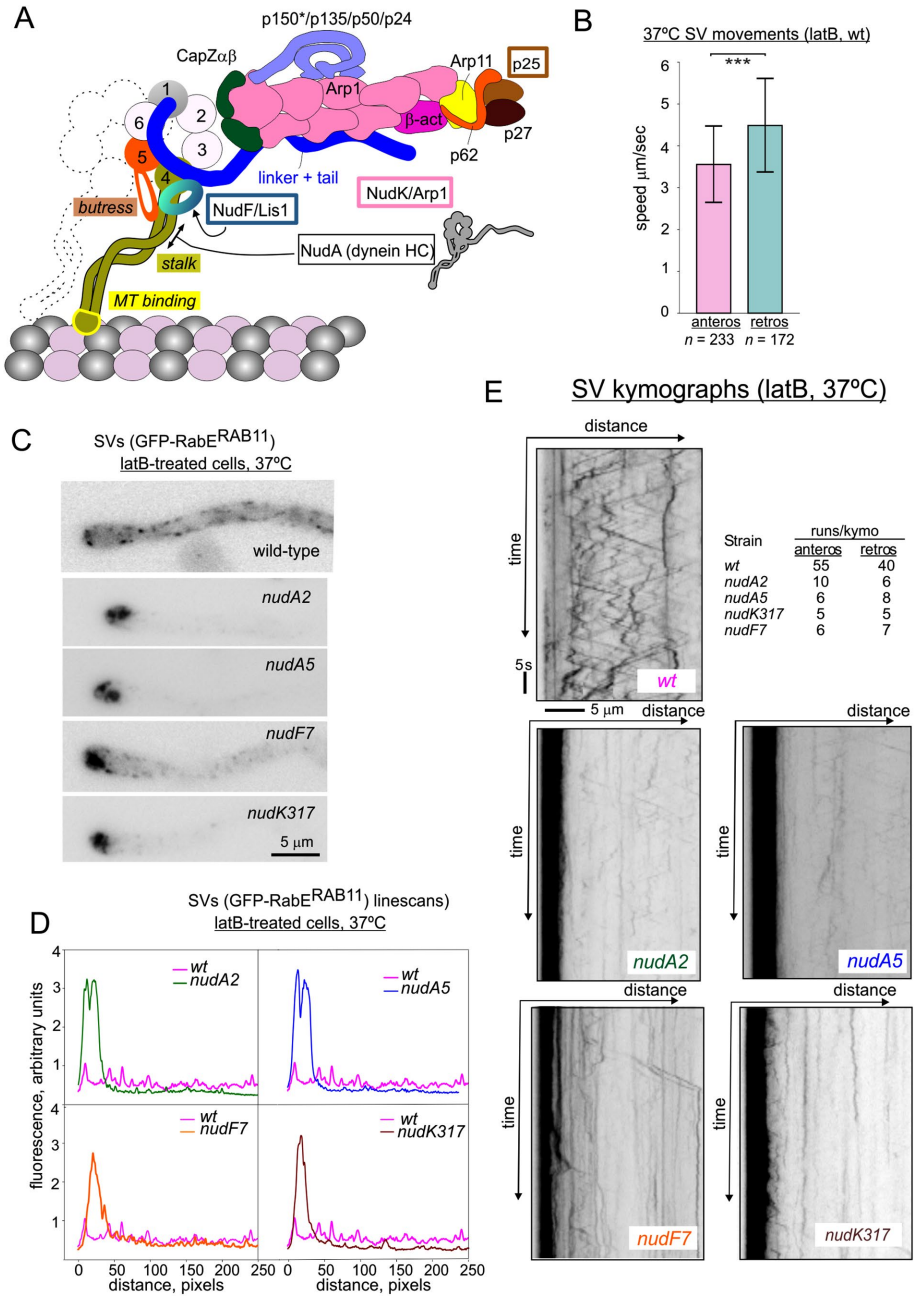

FIGURE 2: Retrograde transport of SVs impeded by mutations affecting key dynein pathway components. (A) Simplified scheme of the cytoplasmic dynein supercomplex. Boxes highlight names of polypeptides affected by mutations used throughout this work. For simplicity, only three protofilaments of a MT are depicted. The different domains in the dynein heavy chain (HC), namely MT binding, stalk, buttress, AAA ATPase rings, linker, and tail, are indicated with different colors (with a gray miniature on the right depicting the whole molecule). Because the biologically active HC is a dimer, the second monomer is indicated with a discontinuous trace. The cartoon, which does not include parts of p150 (indicated by p150*) and does not show polypeptides corresponding to light (LC7, LC8, and Tctex), intermediate (IC), and light intermediate (LIC) dynein chains, emphasizes the accessibility of the p25/p27 dynactin subunits for interactions. The cartoon is based on recent reports and reviews on the dynein supercomplex (Toropova *et al.*, 2014; Chowdhury *et al.*, 2015; Cianfrocco *et al.*, 2015; Schmidt *et al.*, 2015; Urnavicius *et al.*, 2015; Carter *et al.*, 2016). (B) Average speeds of SVs derived from kymographs for 233 anterograde and 172 retrograde SV movements pooled from five wt hyphae treated with latB after cells had been preincubated for 30–60 min at 37°C. Error bars indicate SD. The average values (3.5 ± 0.9 SD and 4.5 ± 1.1 SD µm/s for anterograde and retrograde runs, respectively) were significantly different ($p < 0.0001$) in an unpaired *t* test. (C) Photographs in the GFP channel of hyphal tip cells of the indicated mutant strains expressing GFP-RabE^{RAB11}, treated with latrunculin B after 30–60 min of incubation at 37°C. (D) Line scans traced across the hyphal axis of the cells in C. The same wt control is included in all panels for clarity. (E) Kymographs derived from 22.5-s movies (400 frames/min) using lines traced longitudinally across the 20-µm apicalmost regions of hyphae of the indicated strains. Colors used for the kymograph strain labels match those of the line scans in D. The table summarizes the number of SV movements (runs).

Movies S4 and S5), as expected from the fact that the wt distribution of SVs mainly reflects anterograde transport by kinesin and myosin.

To test whether SVs have the same requirements as EEs to engage dynein, we used *p25Δ* and *hookAΔ mutants* in latB assays. Of note, we observed a stark difference between the two mutants. Contrary to EEs, which remained stalled at the mutant tips (Supplemental Figure S2 and Supplemental Movie S6), SVs of *hookAΔ* cells were shifted to the MT-dependent conveyor belt as in the wt (Figure 3, A and B). When taken together with experiments using dynein pathway mutants (Figure 2), this observation establishes that the dynein-dependent retrograde transport of SVs accumulated at the apex does not require the FHF adaptor complex. In contrast, SVs were detached from the apices of *p25Δ* cells by latB but did not undergo retrograde transport (Figure 3, A and B), remaining stalled in the tips, like EEs (Supplemental Figure S2 and Supplemental Movie S7). Thus the behavior of SVs in *p25Δ* cells resembles that of dynein pathway mutants. We concluded that dynein engagement by SVs requires dynactin p25 but not HookA.

To characterize in greater detail the effects of *p25Δ* and *hookAΔ* on the motility of SVs, we counted the number of RabE^{RAB11} vesicle runs per minute in samples of wt, *p25Δ*, and *hookAΔ* cells treated with latB, using 20-µm-long kymographs starting at the apex (Figure 3B). This quantification yielded similar numbers of anterograde and retrograde runs per wt cell (mean values, ~130 runs/min in each direction; Figure 3C). This traffic was abolished by *p25Δ* (Figure 3, B and C), as expected from the fact that most RabE^{RAB11}-positive membranes were stalled in the *p25Δ* tips (Figure 3A). In marked contrast, *hookAΔ* cells were only moderately affected: the number of runs per cell was reduced by 50% (or even less in the case of anterograde movements) in the *hookAΔ* mutant compared with the wt (Figure 3C). Moreover, the speeds of anterograde and retrograde SV runs (2.2 ± 0.5 SD

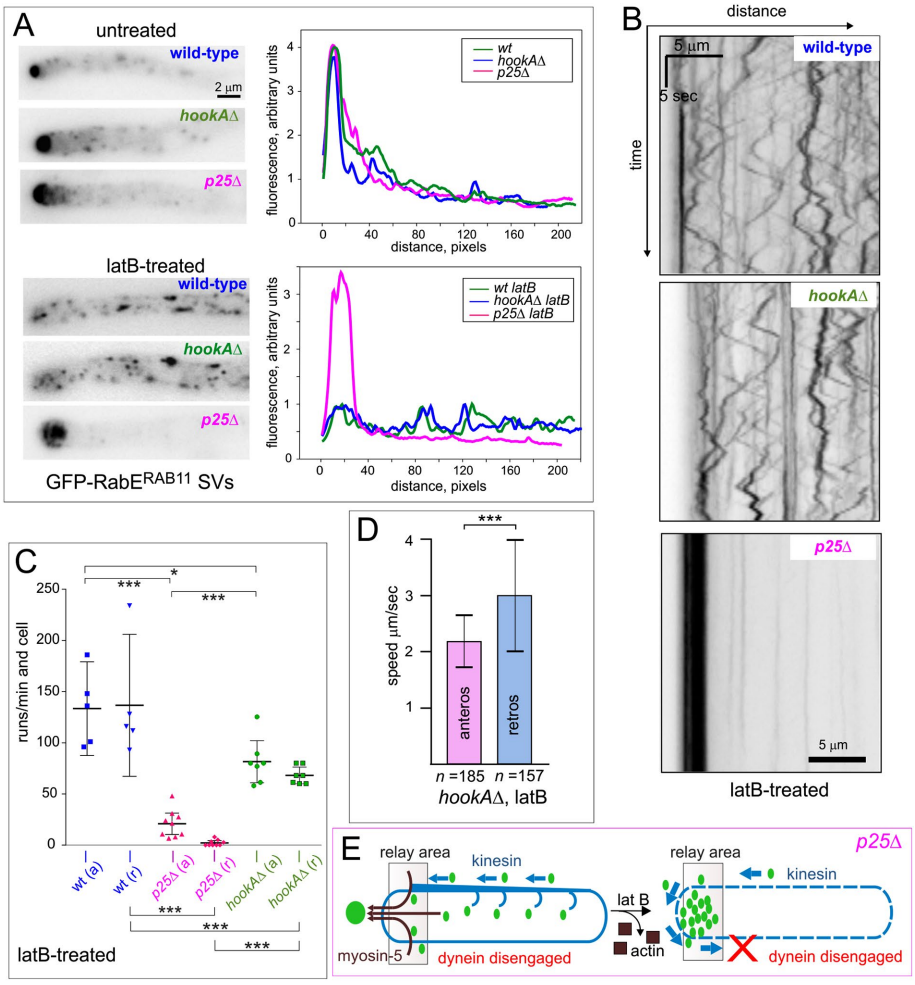

FIGURE 3: Recruitment of the dynein complex to SVs and EEs. (A) Photographs, in the GFP channel, of hyphal tip cells of the indicated mutant strains expressing GFP-RabE^{RAB11}, treated or not with latB at 28°C, and the corresponding line scans. (B) Movement of SVs upon latB treatment: kymographs derived from 15-s movies (400 frames/min) using lines traced longitudinally across the hyphae of strains in A (latB conditions). Colors of the strain labels match those of the bottom line scans in A. (C) Movement of SVs: ~20-µm-long kymographs starting at the apex were used to count manually the number of anterograde (a) and retrograde (r) runs in five wt, nine *p25Δ* and seven *hookAΔ* hyphae treated with latB. Horizontal bars indicate the means, and error bars depict 95% CIs. The different data sets were compared using ANOVA followed by Bonferroni's multiple comparison posttest. ***$p < 0.001$, *$p < 0.05$. (D) Comparison of average speeds of indicated numbers of SVs pooled from kymographs of three *hookAΔ* mutant hyphae treated with latB (note that *p25Δ* mutant cells showed essentially no motility under these conditions). Data sets were compared using an unpaired *t* test with Welch's correction. ***$p < 0.0001$. Here anteros and retros indicate anterograde and retrograde runs, respectively. Error bars indicate SD. (E) In *p25Δ* cells, latrunculin B detaches SVs from the SPK as in the wt, but these SVs are not transferred to the MT conveyor belt because they cannot engage dynein and remain stalled at the tips.

and 3.0 ± 1.0 SD µm/s, respectively; Figure 3D), were slightly reduced relative to the wt (see Figure 1E for the wt at 28°C). These moderate effects of *hookAΔ* on the flux and speed of SVs and the fact that SVs are completely released from the apices by latB strongly argue against a direct involvement of HookA in retrograde transport. Moreover, the fact that in *hookAΔ* cells, RabE^{RAB11} SVs are transferred efficiently to MT-dependent motors rules out the possibility that it is the accumulation of EEs at the tip that actually precludes, due to MT traffic congestion, the dynein-dependent movement of RabE^{RAB11} membranes in the latB-treated *p25Δ* mutant. Therefore we conclude that p25 of dynactin is absolutely required for the association of the dynein complex with both SVs (Figure 3E) and EEs, whereas the HookA/FHF complex adaptor is required for dynein engagement to EEs and dispensable for its engagement to SVs.

The retrograde transport of RabE^{RAB11} SVs observed in latB-treated *hookAΔ* cells establishes that SV motion does not involve hitchhiking on EEs, because EE movement requires HookA. This conclusion is important because in this particular regard, MT-dependent SV traffic differs from that of polysomes, peroxisomes, and lipid droplets, which distribute across hyphal cells by hitchhiking on EEs (Higuchi *et al.*, 2014; Guimaraes *et al.*, 2015; Salogiannis *et al.*, 2016). It is also consistent with our previous observations that SVs do not colocalize with EEs labeled with RabA^{RAB5} or FYVE^{Vps27} (a phosphatidylinositol 3-phosphate–binding duplicated copy of the Vps27 FYVE domain; Pantazopoulou *et al.*, 2014). Finally, the requirement of p25 for the dynein-mediated transport of two different cargoes, EEs and SVs, suggests that p25 facilitates the interaction of dynactin with two different cargo adapters (the FHF complex for EEs and an as-yet-unidentified adaptor for SVs) and/or has a broad role in dynactin function (see the *Discussion*).

kinAΔ impairs the retrograde movement of SVs away from the SPK by causing a dynein deficit at the tips

KinA is required for the transport of dynein to the plus ends of MTs (Zhang *et al.*, 2003). Therefore *kinAΔ* results in deficient supply of dynein to the hyphal tip, which leads to EEs accumulating in this region due to their inability to move away retrogradely (Lenz *et al.*, 2006; Abenza *et al.*, 2009). Similarly, SVs detached by latB from the SPK would be expected to accumulate in *kinAΔ* mutant tips, resembling *nudA*, *nudF*, and *nudK^{ARP1}* heat-sensitive as well as *p25*-null mutant tips. LatB treatment of *kinAΔ* cells expressing GFP-RabE^{RAB11} showed that this is indeed the case (Figure 4A). The penetrance of this phenotype (i.e., the formation of accretions of SVs in the tips of latB-treated *kinAΔ* cells) was nearly complete: 90% (n = 80) of *kinAΔ* tips contained SV aggregates, contrasting with only 6% (n = 124) of tips of similarly treated wt cells. However, inspection of *kinAΔ* aggregates showed that they were generally less bright than those forming in dynein pathway mutants. We also observed this weaker-than-*nud kinAΔ* phenotype with the tip aggregates of EEs (Abenza *et al.*, 2009), which hinted at the possibility that the dynein deficit at the *kinAΔ* tips might not be complete. To address this possibility, we introduced an endogenously tagged *nudA-3xGFP* allele (Egan *et al.*, 2012) into the *kinAΔ* mutant. In the wt, NudA associated with the plus ends of growing MTs, which results in comet-like structures that move toward the tip (Supplemental Movie S8), as

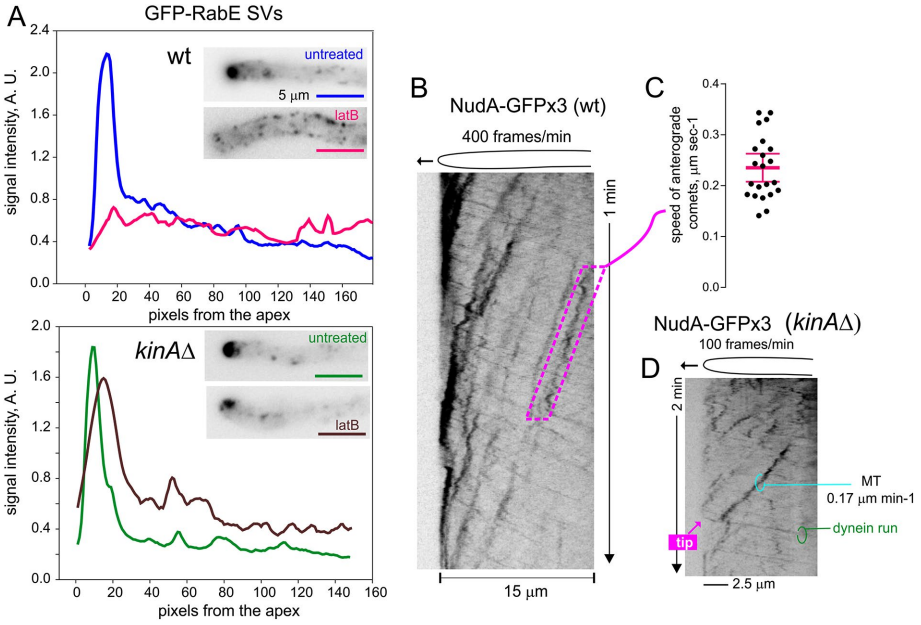

FIGURE 4: Kinesin-1 KinA is important but not essential for dynein localization to the hyphal tips. (A) Photographs in the GFP channel of hyphal tip cells of the indicated mutant strains expressing GFP-RabE^{RAB11} treated or not with latrunculin B at 28°C and the corresponding linescans. (B) Typical kymograph (400 frames/min) depicting the two different classes of movements of NudA-GFPx3 in a wt cell. Anterograde, slower movements correspond to the plus end–tracking activity of NudA and reflect the growth of MTs at the plus ends. The numerous retrograde, faster movements giving rise to faint trajectories reflect the minus end–directed motor activity of dynein. (C) Calculation of the plus-end extension rate of MTs using the NudA-GFPx3 signals (three different hyphae). Mean ± 95% CI. (D) Kymograph of NudA-GFPx3 in a *kinAΔ* cell. Note that the time resolution is one-fourth of that used for B due to markedly lower signal (and thus the slope of the different runs in these images cannot be directly compared). In spite of this, dynein comets arriving at the tip are noticeable, as are fast retrograde dynein runs that depart from the tip region.

described (Xiang *et al.*, 2000; Egan *et al.*, 2012). In addition, retrograde trajectories representing the motor's minus end–directed movement were noticeable in the movies. Kymographs captured both the stronger signals of the less abundant and slower anterograde dynein comets and the numerous, much faster and weaker signals resulting from retrograde minus end–directed departures (Figure 4B). The average speed of anterograde NudA comets was 0.23 ± 0.06 SD µm/s (Figure 4C). This speed fits well with the previously reported MT growth rate determined with green fluorescent protein (GFP)–tagged α-tubulin (GFP-TubA) in *A. nidulans* (Han *et al.*, 2001; 13.8 µm/min with NudA vs. 13.7 µm/min with TubA), confirming that comets indeed reflect the accumulation of NudA at the plus-ends of MTs.

We next observed NudA in *kinAΔ* cells by time-lapse imaging, which confirmed that NudA signals are progressively weaker toward the tip, in agreement with the demonstrated involvement of KinA in determining NudA polarization (Zhang *et al.*, 2003, 2010; Lenz *et al.*, 2006; Egan *et al.*, 2012). However, although observations were limited by the long exposure times required, we documented both the arrival of faint comets to the tip and the departure of rapidly moving retrograde dynein signals from this region (Supplemental Movie S9). These fast dynein runs were captured by kymographs (Figure 4D). The fact that NudA comets reach the tip region (Figure 4D) strongly indicates that the robust MT plus end–tracking capability of NudA provides a mechanism to deliver dynein NudA to the plus end–rich tips. This mechanism appears to be largely, but not completely, dependent on KinA/kinesin-1 (Zhang *et al.*, 2003; Cianfrocco *et al.*, 2015).

Evidence that KinA (kinesin-1) is the main kinesin cooperating with MyoE (myosin-5) in SV transport

A role for kinesin(s) in the anterograde transport of SVs was inferred from several observations (Pantazopoulou *et al.*, 2014): 1) MT depolymerization markedly decreases the apical accumulation of SVs in the wt and completely prevents it in a *myoEΔ* mutant; 2) kymograph analyses revealed a class of SV anterograde trajectories moving over several micrometers with uniform speeds toward the wt SPK, consistent with transport along stiff MTs rather than along flexible actin filaments; and 3) *myoEΔ,* albeit debilitating, does not impede growth, and indeed the presence of RabE^{RAB11} SVs delivered by active transport (i.e., with speed and directionality incompatible with diffusive mechanisms) to the apical dome of *myoEΔ* cells has been documented (Pantazopoulou *et al.*, 2014). We confirmed that this transport is actually MT mediated by coimaging GFP-RabE^{RAB11} SVs with GFP-labeled MTs in *myoEΔ* cells (Figure 5A). Supplemental Movie S10 is a composite showing a GFP-MT cell alongside a GFP-MTs-and-GFP-SVs doubly labeled cell to illustrate that the fainter MTs do not interfere with the visual tracking of SVs and that the latter can be distinguished moving on MTs. Therefore, considering the orientation of tip MTs, the contribution of MT-mediated transport to SV delivery must involve kinesin(s). However, the identity of the kinesin(s) is currently unknown.

We approached this problem genetically, exploiting the phenotypes of null mutants in motor-encoding genes. Note that kinesin and myosin-5 activities cooperate to deliver SVs, but the motors do not strictly act in parallel. Kinesin(s) move vesicles toward the tip but cannot compensate for the absence of MyoE because MT transport cannot focus SVs at the growing apex (Taheri-Talesh *et al.*, 2012; Pantazopoulou *et al.*, 2014). Thus SV delivery is very inefficient in *myoEΔ* cells. In contrast, MyoE transport is expected to compensate for the absence of the kinesin(s) because actin cables radiating from the apex (and therefore the activity of MyoE motors) stretch backward into the subapical region in which TGN cisternae (the origin of SVs) are highly abundant (Pantazopoulou and Peñalva, 2009), making the contribution of kinesin relatively less important. In such a scenario, combining SV kinesin and myosin-5 null mutations should preclude growth, leading to lethality. A clear candidate for an SV kinesin is KinA because a *kinA* disruption allele (*kinA::pyr-4*; Requena *et al.*, 2001) is virtually lethal when combined with MyoE (myosin-5) down-regulation (Zhang *et al.*, 2011a). Given the importance of this observation, we constructed complete deletion alleles of *kinAΔ* (removing kinesin-1) and *uncAΔ* (removing the endosomal UncA kinesin-3; Zekert and Fischer, 2009) to revisit their genetic interactions with a null *myoEΔ* allele (Taheri-Talesh *et al.*, 2012).

We first studied the effects of the mutations in colony growth on solid medium. Compared to the strong *myoEΔ* colony growth defect, *kinAΔ* and *uncAΔ* single-deletion mutations had a minor negative effect on growth, although that of *kinAΔ* was more

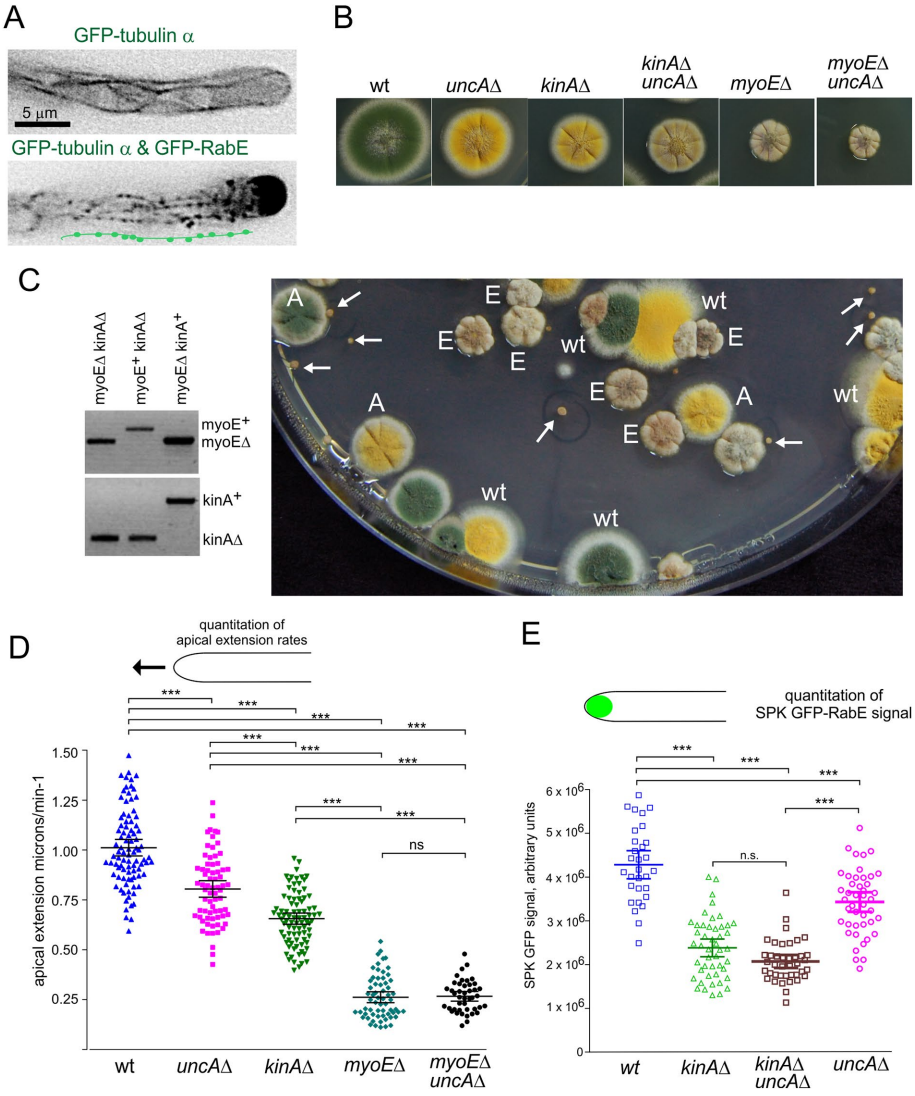

FIGURE 5: Genetic data strongly suggest that kinesin-1 (KinA) cooperates with myosin-5 (MyoE) in exocytosis. (A) *myoEΔ* hyphal tip cells expressing GFP–α-tubulin alone (as control) or coexpressing GFP–α-tubulin and GFP-RabE^{RAB11} to detect MTs and SVs, respectively. The double-labeled cell image is overcontrasted to show SVs aligned along MTs. Images were treated with the unsharp filter of MetaMorph. (B) Colony-growth phenotypes of motor mutant strains at 37°C. Colonies of indicated genotypes were ordered from left to right according to the growth impairment caused by the single- or double-null alleles. Note that all mutant motor strains carry *yA2* resulting in yellow conidiospores (wt color is green) and that *uncAΔ* and *myoEΔ* show a weak, yet noticeable synthetic negative interaction. (C) A double *myoEΔ kinAΔ* mutation is virtually lethal. Left, diagnostic PCRs used to genotype deletion alleles. Right, progeny of a heterozygous cross between *myoEΔ* and *kinAΔ* parental strains plated on rich medium and incubated at 37°C. The minute colonies indicated with white arrows were diagnosed as *myoEΔ kinAΔ* double mutants by PCR. A and E indicate *kinAΔ* and *myoEΔ* progeny, respectively; wt is *kinA*$^+$ *myoE*$^+$ (yellow or green conidiospores). (D) Quantitation of apical extension rates in the wt and indicated single- and double-mutant strains. Strains were cultured at 29.5 ± 0.5°C on the microscope stage before collection of time stacks using Nomarski optics, which were used to deduce apical extension rates of individual cells. Scatter plots show mean ± 95% CI. The different data sets were compared by ANOVA followed by Bonferroni's multiple comparison posttest. ***$p < 0.001$; ns, nonsignificant. (E) Quantitation of the GFP-RabE^{RAB11} fluorescence signal in the SPKs of the wt and indicated mutant strains. Scatter plots also display mean ± 95% CI. The data sets were compared by ANOVA followed by Tukey's multiple comparison posttest. ***$p < 0.001$; n.s., nonsignificant.

marked (Figure 5B). Combining *myoEΔ* with *uncAΔ* only slightly exacerbated the growth impairment caused by *myoEΔ* alone (Figure 5B). In sharp contrast, the double *myoEΔ kinAΔ* mutant combination, obtained from a heterozygous cross, showed strong negative additivity, leading to barely visible colonies that could not be further subcultured (arrowed on Figure 5C). Combining *myoEΔ* with *kipAΔ* (removing the kinesin KipA involved in growth directionality determination; Konzack *et al.*, 2005) did not have any effect (unpublished data). Therefore genetic data strongly suggest that KinA is the major kinesin cooperating with MyoE to deliver SVs to the apex. To estimate quantitatively the contributions of motors to exocytosis, we determined by time-lapse microscopy actual apical extension rates of individual wt and mutant tip cells cultured in minimal medium, using inverted microscope chambers incubated at 29.5 ± 0.5°C. Under these conditions, wt cells grew at 1.01 ± 0.2 μm/min (mean ± SD), whereas *uncAΔ* cells grew significantly more slowly than the wt, at 0.8 ± 0.17 μm/min (~20% reduction; Figure 5D). The *kinAΔ* tips grew even more slowly (at 0.66 ± 0.13 μm/min, ~35% reduction), and *myoEΔ*, which shows a strong colony growth defect (Figure 5, B and C; Taheri-Talesh *et al.*, 2012), reduced the actual apical extension rate by ~75% (to 0.26 ± 0.1 μm/min; Figure 5D). Thus these differences roughly resemble those observed in colony growth tests. However, these assays could not discriminate the minor differences in (poor) growth detected by colony tests between single *myoEΔ* and double *myoEΔ uncAΔ* cells.

Attempting to correlate the apical extension rate defects with exocytic traffic impairment, we tested by time-lapse imaging whether the absence of either KinA or UncA affected the steady-state accumulation of RabE^{RAB11} SVs at the SPK. Neither *uncAΔ* nor *kinAΔ* impeded such accumulation. However, we noticed both reduced compactness and apparently reduced brightness specifically in the SPK of *kinAΔ* hyphae. Prompted by these observations, we determined the fluorescence intensity of GFP-RabE^{RAB11} in the SPKs of the wt and kinesin mutant strains (Figure 5E), which confirmed that the *kinAΔ* SPK shows half the fluorescence of the wt, whereas the *uncAΔ* SPK was much less, yet significantly affected, in agreement with colony growth and apical extension rate tests. The fact that the double *kinAΔ uncAΔ* mutant was not significantly different from the single *kinAΔ* mutant (Figure 5E) further indicates that KinA plays the major role in the transport of SVs.

Rigor kinesin mutants reveal a direct role of KinA in the anterograde transport of RabE^{RAB11} SVs

A potential drawback of the foregoing experiments is that in view of its numerous physiological roles in MT transport, ablation of

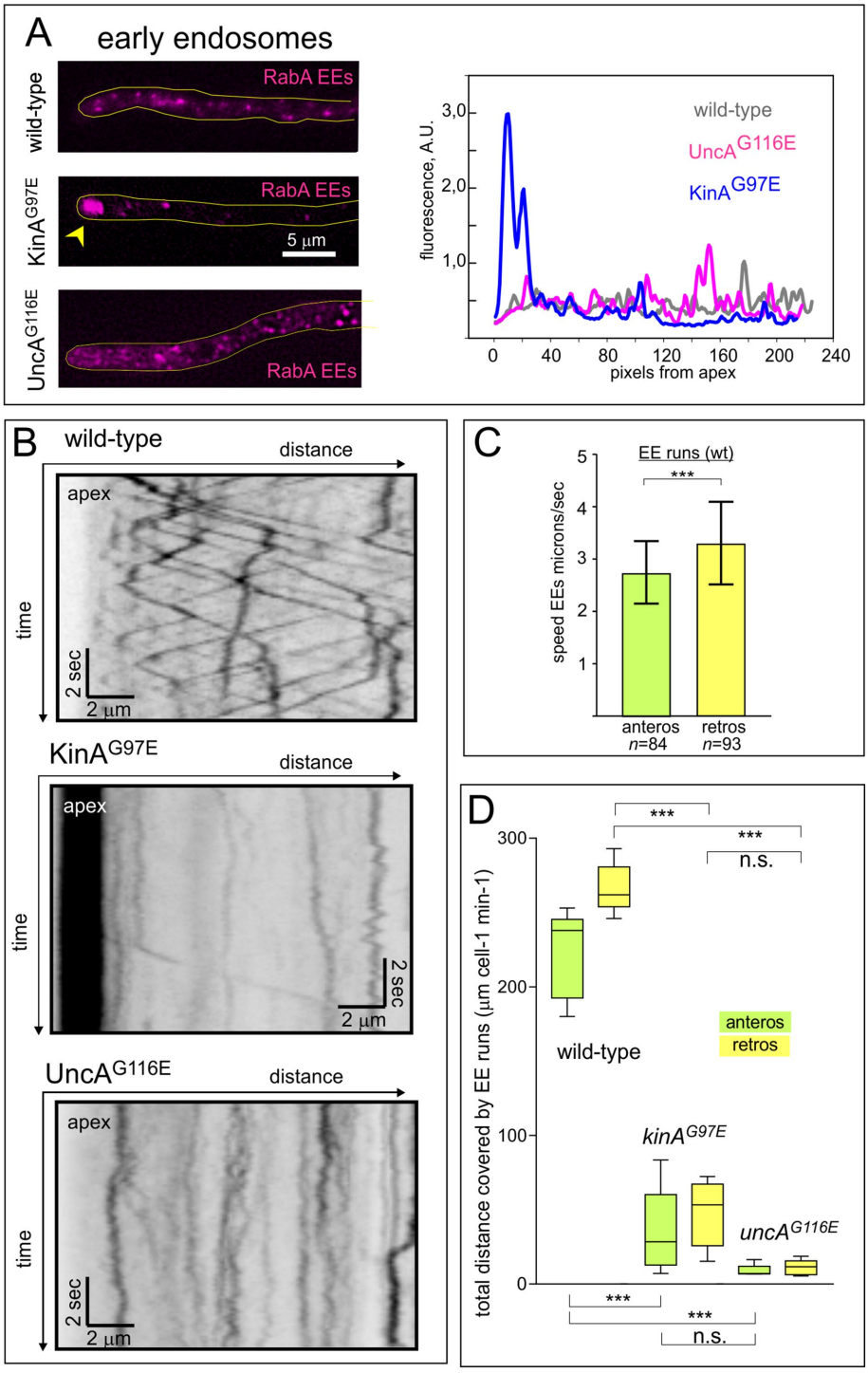

FIGURE 6: Rigor mutations affecting kinesin-1 and kinesin-3. (A) Localization of EEs labeled with RabA (RAB5) in the wt and in cells expressing rigor mutant kinesins: examples and line scans. The yellow arrowhead points at the tip accumulation of EEs in the *kinA*^{G97E} hypha. (B) Kymographs derived from time stacks of RabA^{RAB5} EEs images (400 frames/min) comparing the two different ways in which kinesin rigor mutations eliminate the movement of EEs. (C) Calculation of average speeds deduced for EE movements determined using 20-µm-long kymographs starting at the apex (four hyphae). Average speeds of anterograde and retrograde EE runs were significantly different in an unpaired *t* test ($p < 0.0001$). Error bars represent SD. (D) Quantitative estimation of EE motility. The box diagrams (median with Tukey's bars) show the total (accumulated) distance covered by anterograde or retrograde EE runs that were captured by 20-µm-long kymographs starting at the apex of five 5 hyphae for each genotype. The different data sets were compared by ANOVA followed by Bonferroni's multiple comparison posttest. ***$p < 0.001$; n.s., nonsignificant.

kinesin-1 might affect growth indirectly, as illustrated by the described *kinAΔ* defect on dynein localization. For example, *kinA* disruption stabilizes MTs (Requena *et al.*, 2001). More-stable MTs would not affect transport per se, but MT and actin transport act in concert (the tip growth apparatus; Taheri-Talesh *et al.*, 2008), and thus a hyperstable MT network could affect the network of AFs converging at the apex. However, the MyoE steady-state localization to the apex, dependent on this network, is not altered by *kinAΔ* (Supplemental Figure S3), arguing strongly against this possibility. Another possibility would be that given that *U. maydis* kinesin-1 is required for efficient MT bundling (Straube *et al.*, 2006), *kinAΔ* weakens MT bundles at the tip, creating a gap between MTs and the cortex that debilitates MT-mediated exocytosis, making MyoE essential. This possibility was discarded after observing, in *kinAΔ* tips, GFP-labeled MTs, which are clearly capable of reaching the apical dome (Supplemental Figure S4).

In view of the foregoing considerations, we sought evidence supporting a direct role of KinA in SV transport. We used gene replacement to construct mutant alleles encoding UncA^{G116E} and KinA^{G97E} rigor kinesins (Zekert and Fischer, 2009). These substitutions in the respective Walker motifs do not preclude MT binding but disable motor activities due to deficient ATP cycles. First, we characterized the efficacy of the rigor mutations by imaging the behavior of EEs labeled with mCherry-RabA^{RAB5} by time-lapse microscopy. In the wt, EEs show an even distribution across hyphae (Figure 6A) and display characteristic anterograde and retrograde movements powered by kinesins and dynein (Abenza *et al.*, 2009; Zekert and Fischer, 2009; Zhang *et al.*, 2011b, 2014; Egan *et al.*, 2012; Yao *et al.*, 2014, 2015; Xiang *et al.*, 2015). These movements can be captured by kymographs (Figure 6B). We deduced from these kymographs the average anterograde and retrograde speeds of EEs in the wt, which were 2.7 ± 0.6 SD and 3.3 ± 0.8 SD µm/s, respectively (Figure 6C). This significant difference ($p < 0.001$ in unpaired *t* test) had not been detected in previous works (including our own; Abenza *et al.*, 2009; Egan *et al.*, 2012), which is possibly related to improvements in the in vivo imaging of mCherry-RabA^{RAB5} (see *Materials and Methods*). Given the polarity of MTs in the tip-proximal region, these data suggest that dynein may be more efficient than kinesin-3 in the overall speed output at which motor teams propel EE movement. Physiological speeds reflect the influence of numerous factors besides the motors'

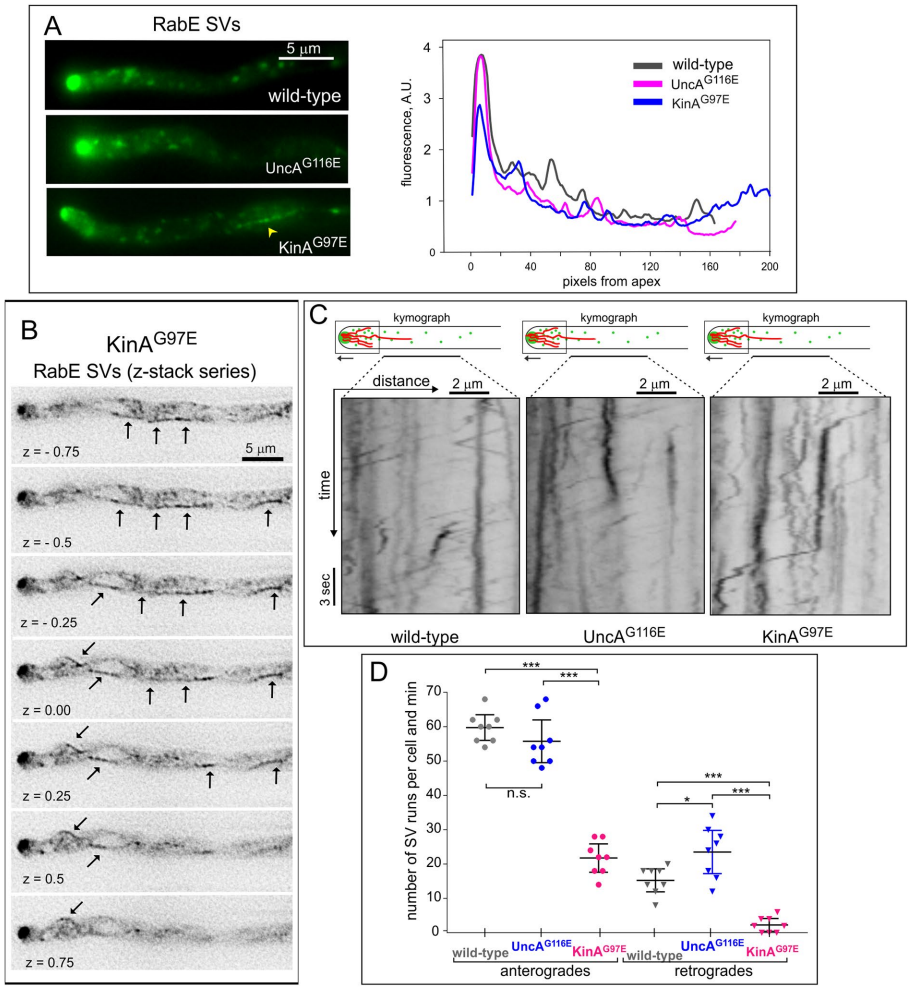

FIGURE 7: Localization and trafficking of GFP-RabE^{RAB11} in cells expressing rigor kinesins. (A) Localization of SVs labeled with GFP-RabE^{RAB11} in the wt and in cells expressing rigor mutant kinesins: examples and line scans. The yellow arrowhead points at a MT decorated with rigorously bound SVs in the *kinA^{G97E}* hypha. (B) Wide-field sections derived from a *z*-stack of images of a *kinA^{G97E}* cell showing GFP-RabE^{RAB11} SVs decorating MTs (indicated with arrows). *Z*-step, 0.25 µm. (C) Anterograde runs attributable to kinesin-1 in subapical regions of hyphae. Time stacks of images of wt and mutant hyphae were used to construct kymographs. To minimize the effect of anterograde AF-mediated transport, these kymographs were drawn to detect the flux of vesicles across 10-µm-long apex-proximal regions that excluded the 2- to 4-µm apicalmost areas of hyphae. Faint anterograde runs, attributable to MT transport, were conspicuous in wt and *uncA^{G116E}* but not in *kinA^{G97E}* hyphae. (D) Flux of anterogradely and retrogradely moving SVs in regions described in C in eight hyphae for each genotype. The total number of runs per hyphae and minute was determined by visual inspection of kymographs. Runs were classified as anterograde or retrograde and plotted as means with 95% CIs. The different data sets were compared by ANOVA followed by Bonferroni's multiple comparison posttest. ***$p < 0.001$, *$p < 0.05$; n.s., nonsignificant.

biochemical activity, and these factors could include the balance between opposing motor teams binding to the same organelle. Of note, in *U. maydis*, a single dynein dimer can support retrograde EE transport, whereas anterograde movement requires several kinesin units (Schuster *et al.*, 2011).

Kymographs were also used to estimate EE motility in any given cell as the total distance covered by EE runs per unit time (Figure 6D). Both UncA^{G116E} and KinA^{G97E} affected the motility of EEs markedly (Figure 6, B and D). In UncA^{G116E} cells, EEs were uniformly distributed along the hyphae as in the wt (Figure 6A, line scans), but in sharp contrast with the latter, they were completely immotile (Figure 6, B and D), in agreement with reports that UncA is the principal kinesin powering EEs (Wedlich-Soldner *et al.*, 2002; Zekert and Fischer, 2009; Egan *et al.*, 2012). In contrast, KinA^{G97E} cells were largely devoid of EE movement (Figure 6, B and D) because EEs accumulated in the tip (Figure 6A, yellow arrowhead), indicating that EEs arrive normally at this region (KinA does not move EEs) but are inefficiently transported retrogradely due to local dynein deficit resulting from *kinA^{G97E}*. These dynamic phenotypes are better displayed as movies. Supplemental Movie S11 shows the almost complete absence of EE movement resulting from *uncA^{G116E}*, and Supplemental Movie S12 shows that *kinA^{G97E}* EEs accumulate in the slightly subapical dynein-loading zone (Lenz *et al.*, 2006). We concluded that the kinesin alleles behaved as expected for rigor mutations.

We next studied the localization of RabE^{RAB11} SVs in hyphae expressing UncA^{G116E} or KinA^{G97E}, which was essentially wt, that is, apical accumulation of SVs with some labeling associated with TGN puncta (Figure 7A). However, inspection of time-lapse movies (Supplemental Movie S13 compares the wt and KinA^{G97E} hyphae) suggested that the KinA^{G97E} SPK was less compact. In addition, KinA^{G97E} hyphae displayed two clear phenotypes with regard to SV transport. The first was that immotile SVs often decorated MTs in a beads-on-a-string manner. Supplemental Movie S13 (Figure 7A) shows the behavior over time of these rigorously bound SVs. Figure 7B shows consecutive sections of a *z*-stack showing MT tracks decorated with rigorously bound SVs all along a hyphal tip cell. These data strongly indicate that KinA^{G97E} motors bind to SVs and that these motors loaded with SVs are able to bind MTs but are unable to move. The second phenotype was revealed after tracking movement of SVs with kymographs. It is important to note that both kinesin(s) and MyoE cooperate in the anterograde transport of SVs to the SPK, and thus, in cells that have not been treated with latB to remove the MyoE component of transport, anterograde movements detected by kymographs can be mediated by either MT or actin motors, which hampers quantitative analyses of MT transport. Attempting to reduce the relative weight of actin transport, we estimated the flux of vesicles across a linear 10-µm region that excluded the tip (i.e., 2- to 4-µm region proximal to the apex). In addition, by eliminating the highly fluorescent SPK region from our analyses, we improved detection of the faint runs that we attribute to MT-mediated events (Pantazopoulou *et al.*, 2014). Kymographs of wt and *uncA^{G116E}* cells indeed revealed faint anterograde RabE^{RAB11} runs of similar and uniform speeds in these subapical regions, consistent with kinesin-mediated transport (Figure 7C). By counting these runs, we determined that the flux of anterograde SVs that move across 10-µm-long subapical regions was 55 runs/min in the wt. This flux

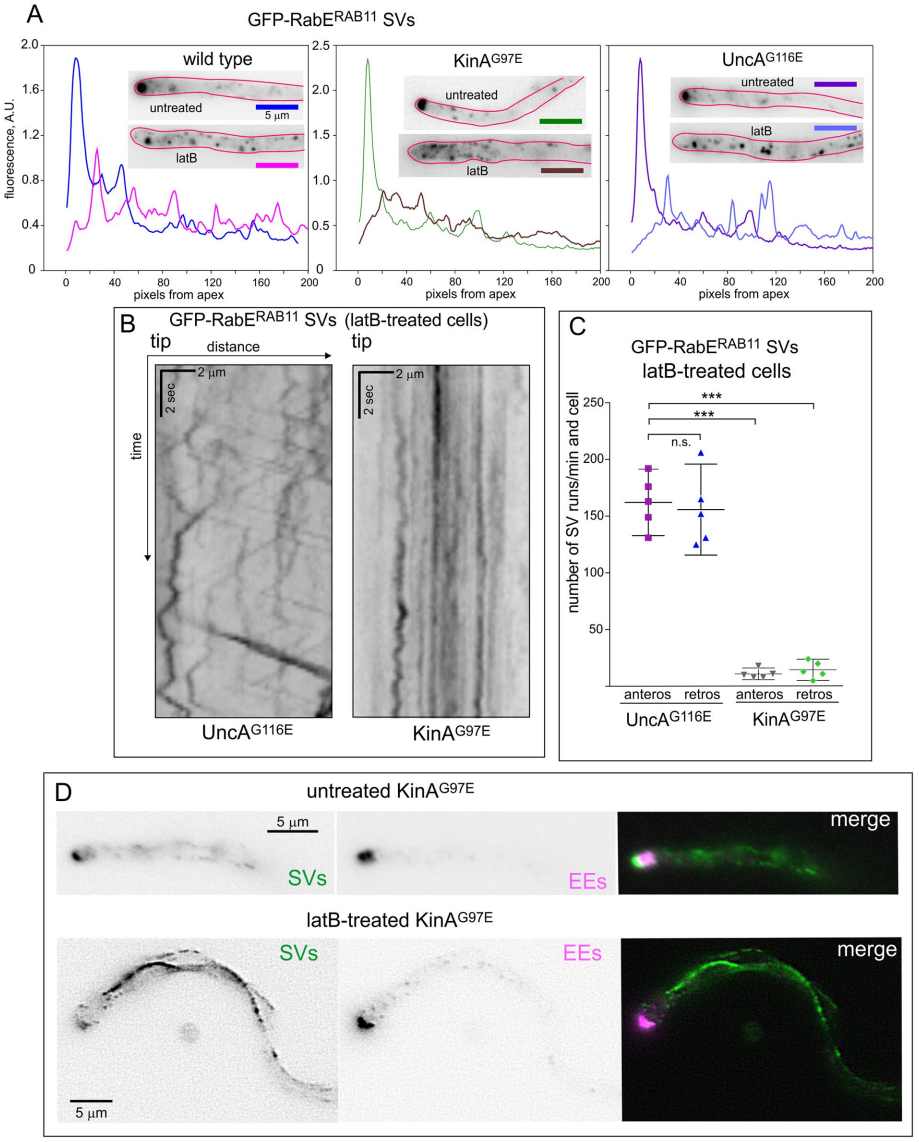

FIGURE 8: SVs rigorously bound by KinA^{G97E} massively decorate MTs after latrunculin B treatment. (A) Localization of SVs labeled with GFP-RabE^{RAB11} in the wt and in cells expressing rigor mutant kinesins with and without latB treatment. (B) Kymographs (10 µm long, starting at the apex) derived from time stacks of GFP-RabE^{RAB11} images obtained from *kinA^{G97E}* and *uncA^{G116E}* cells treated with latB (600 frames/min). (C) Flux of anterograde and retrograde runs in regions described in B in five latB-treated hyphae for each genotype. The total number of runs per hypha and minute was determined by manual tracking on kymographs. Runs were classified as anterograde or retrograde and plotted as means with 95% CIs. The different data sets were compared by ANOVA followed by Tukey's multiple comparison posttest. ***$p < 0.001$; n.s., nonsignificant. (D) KinA^{G97E} cells coexpressing mCh-RabA^{RAB5} to label EEs and GFP-RabE^{RAB11} to label SVs. In the untreated KinA^{G97E} control, SVs accumulate in the SPK and EEs in a slightly subapical aggregate. LatB treatment of KinA^{G97E} cells shifts SVs from the SPK to MTs, which are conspicuously decorated with rigorously bound vesicles. Note that the tip accumulation of EEs is not dispersed by actin depolymerization (see also Supplemental Movies S15 and S16).

was not significantly different in *uncA^{G116E}* cells but was reduced by approximately threefold in *kinA^{G97E}* ones (Figure 7D; note that some of these anterograde runs in *kinA^{G97E}* might still be attributable to myosin). Retrograde runs were markedly less abundant than anterograde ones in the wt, slightly increased by *uncA^{G116E}*, and virtually eliminated by *kinA^{G97E}* (an observation that can be explained by the dynein deficit near the tip in this mutant). In summary, all of the foregoing observations imply that UncA moves EEs (but not SVs), whereas KinA powers the anterograde transport of SVs toward the tip.

Our experiments revealing weak effects of *uncAΔ* in apical extension and SPK brightness (Figure 5, D and E) suggested that UncA might play an ancillary role in anterograde SV transport. However, the finding that *uncA^{G116E}* did not reduce the anterograde transport of SVs (Figure 7D) argues strongly against this possibility. Thus the foregoing *uncAΔ* phenotypes are perhaps attributable to an overall defect in EE transport resulting from *uncAΔ*. Moreover, if kinesin-1 (KinA) is the only MT motor mediating anterograde SV transport, the *myoEΔ kinA^{G97E}* combination should be as debilitating as the nearly lethal *myoEΔ kinAΔ* combination. Indeed, the progeny of a heterozygous cross germinated in microscopy wells contained ascospores that gave rise to morphologically abnormal abortive germlings resembling those seen when *myoE* was down-regulated in a *kinAΔ* background (Supplemental Figure S5; Zhang *et al.*, 2011a). Hence the genetic interaction between KinA and MyoE involves the cargo-powering role of the kinesin. Taken collectively, all the foregoing data strongly indicate that KinA is the principal kinesin cooperating with MyoE in the anterograde transport of SVs.

F-actin depolymerization shifts RabE^{RAB11} SVs to MTs decorated by rigor KinA^{G97E}

Rigor MTs decorated with SVs in KinA^{G97E} hyphae abounded in regions located far from the apex but were sparser near the tips. This suggested that their detection in tip-proximal regions, in which actin transport is vigorous, might be hindered by the activity of MyoE, which could possibly snatch SVs rigorously bound to MTs and deliver them to the apex. Moreover, because in the steady state, the majority of SVs concentrate in the SPK due to myosin-5 transport, we hypothesized that MT decoration by rigor SVs would be markedly more abundant after releasing the SPK SVs from actin. To test this prediction, we treated cells with latB. Control experiments using EEs labeled with mCh-RabA^{RAB5} established that EEs moved bidirectionally in the wt, were immotile in the UncA^{G116E} mutant, and accumulated in tips in the KinA^{G96E} mutant (Supplemental Figure S6), as in untreated cells

We next focused on SVs. As in the wt, in both *kinA^{G97E}* and *uncA^{G116E}* cells, latB dissipated the SPK accumulation of SVs, which redistributed across hyphae (Figure 8A). In *uncA^{G116E}* cells, SVs underwent bidirectional movements similarly to those in the wt (Figure 8B). Indeed, when we determined the number of vesicle

runs per minute captured by kymographs in the apicalmost 20 µm of *uncA*^{G116E} hyphae, we counted 162 ± 11 anterograde and 156 ± 14 (mean ± SE) retrograde runs per cell (Figure 8C). These figures are similar to those noted for the wt (Figure 3C). The high motility displayed by SVs in *uncA*^{G116E} cells contrasts sharply with the complete absence of EE motility caused by this mutation (Figure 6, B and D; Supplemental Figure S6 and Supplemental Movie S14), implying that UncA moves EEs but not SVs.

The behavior of SVs in *kinA*^{G97E} cells treated with latB was remarkable. *kinA*^{G97E} prevented SV movement, reducing the number of SV runs per cell to almost negligible values (<15 anterograde or retrograde runs per minute per cell) compared with *uncA*^{G116E} (and to the wt; see earlier discussion; Figure 8, B and C). This occurred because in *kinA*^{G97E} cells, SVs released by latB were sequestered by MTs, which were very conspicuously decorated with vesicles, such that within <30 min after addition of latB, essentially all of the RabE^{RAB11} fluorescence was seen on MTs (Figure 8D). Therefore the inability of RabE^{RAB11}SVs to move cannot result from their incapacity to productively meet and engage rigor KinA^{G97E}. In sheer contrast, EEs accumulate in the tips of this mutant (Figure 8D) and do not decorate MTs. Supplemental Movie S15 further shows that KinA^{G97E} SVs do not move, as expected if they were attached to MTs by means of the rigor kinesin. Such inability is unlikely to result from a traffic jam caused by the KinA^{G97E} rigor kinesin, as UncA^{G116E} did not cause the same effect.

Supplemental Movie S16 visually summarizes the effects of latB on SVs in *kinA*^{G97E}, *uncA*^{G116E}, and wt cells. These effects and the genetic analyses in Figure 5 strongly support the contention that RabE^{RAB11} SVs are loaded mostly, if not exclusively, with KinA, strongly indicating that it is this kinesin-1 that mediates the MT-dependent component of their anterograde transport.

DISCUSSION

Many subcellular membranous structures move on MTs and AFs. It is of general interest to understand the mechanisms by which kinesin, myosin-5, and dynein acting on the same cargo coordinate their action, as well the molecular codes by which motors discriminate their physiological cargoes among the lavish diversity of compositionally different intracellular membranous structures (Akhmanova and Hammer, 2010; Fu and Holzbaur, 2014).

Here we studied the long-range transport of *A. nidulans* RabE^{RAB11} SVs to the hyphal apex, which involves kinesin and myosin-5 activities (Pantazopoulou *et al.*, 2014). We establish that kinesin-1 (KinA) is the principal and perhaps the only kinesin powering the MT component of anterograde SV transport, whereas kinesin-3 (UncA) does not play an important role. Thus, according to the current model, SVs would move from tip-distal to tip-proximal regions with MTs/kinesin-1 and would be transferred to AFs/myosin-5 as they arrive to the proximity of the apex. Motor switching at the intersection between actin and MT tracks depends on which set of motors generates the greatest force (Schroeder *et al.*, 2010). We speculate that SVs switch from kinesin-1 to myosin-5 as they reach the region where the AF network originating at the apex becomes denser, thereby increasing the overall performance of myosin-5 motors. Interplay between myosin-5 and kinesin-1 in exocytic transport is evolutionarily conserved. The nonmotile *Saccharomyces cerevisiae* kinesin-1–like protein Smy1 interacts with, and improves the processivity of, myosin-5 acting on SVs by tethering cargo to actin bundles (Hodges *et al.*, 2009). Smy1 transported with SVs by myosin-5 to the sites of exocytosis regulates actin cable stability and dynamics (Chesarone-Cataldo *et al.*, 2011) and, strikingly, Smy1 additionally enhances the association of yeast myosin-5 with SVs by reinforcing the interaction of the motor with the exocytic RAB Sec 4 (Lwin *et al.*, 2016).

It is worth noting that besides powering the final stage of transport, MyoE^{MYO5} also focuses SVs at the apex. Therefore the MT and actin pathways do not act in parallel, as kinesin-1–based transport cannot perform the focusing step, explaining why *myoEΔ* results in markedly defective apical extension, even though kinesin-1 can support exocytosis by way of the MTs that contact the apical dome. Our model also explains why kinesin-1 SV transport is much less important than MyoE transport: a large proportion of the otherwise strongly polarized TGN cisternae fall within the distance covered by actin cables and thus within the domain of action of MyoE. Our findings are also consistent with the report that KinA is involved in the transport of chitin synthases to the hyphal tip (Takeshita *et al.*, 2015). A recent landmark study with *U. maydis* characterized a class of secretory vesicles codelivering cell wall–synthesizing enzymes to the plasma membrane that is dependent on kinesin-1 and myosin-5 (Schuster *et al.*, 2016).

Cytoplasmic dynein consisting of a dynein motor complex and a cofactor dynactin complex is an ~2.5-MDa minus-end MT motor of remarkable complexity (Chowdhury *et al.*, 2015; Cianfrocco *et al.*, 2015; Urnavicius *et al.*, 2015). We established beyond doubt that *A. nidulans* SVs engage dynein/dynactin, as previously suggested by the finding that a proportion of them undergo retrograde movement once they arrive at the SPK (Pantazopoulou *et al.*, 2014). This retrograde movement is conspicuously uncovered after removing with latB the paramount masking activity of AF-based anterograde transport/capture of SVs. We exploited this feature to demonstrate that the retrograde transport of SVs indeed depends on the dynein motor heavy chain, the dynein regulator NudF^{LIS1}, and the integrity of the dynein adaptor dynactin. The mechanisms by which dynein specifically recognizes its numerous membranous cargoes are being intensively studied. Many cargoes exploit RAB effectors acting as adaptors to recruit the motor, with the RAB determining membrane specificity. For example, Golgi cisternae use RAB6 and its effector Bicaudal to bind dynactin (Hoogenraad *et al.*, 2001; Urnavicius *et al.*, 2015), perinuclear recycling endosomes use RAB11 and its effector FIP3 to bind the dynein light intermediate chain (Horgan *et al.*, 2010), and late endosomes use RAB7 and its effectors RILP and ORP1L to bind p150^{Glued} in dynactin (Johansson *et al.*, 2007) and, in the case of RILP, also the dynein light intermediate chain (Scherer *et al.*, 2014). The pointed-end complex capping the dynactin filament and consisting of Arp11, p62, p27, and p25 (Eckley *et al.*, 1999) is accessible in the dynein–dynactin structure to interact with cargo adaptors without interfering with the motor's activity (Chowdhury *et al.*, 2015; Urnavicius *et al.*, 2015), contributing a cargo entry site alternative to p150^{Glued}.

Studies with *U. maydis* and *A. nidulans* led to the identification of the FTS/Hook/FHIP (FHF) complex on endosomes and of p25 in the pointed-end complex of dynactin as key players in the recruitment of dynein by EEs (Zhang *et al.*, 2011b, 2014; Bielska *et al.*, 2014; Yao *et al.*, 2014; Xiang *et al.*, 2015). The role of Hook proteins in dynein engagement was inferred from the accumulation of EEs unable to move retrogradely in the tips of cells carrying null *hook* mutations. Our studies with mutations affecting the dynein pathway showed that dynein inactivation in cells devoid of AFs led to the accumulation of SVs stalled in the tip region, providing a scorable assay for dynein function similar to that based on EEs. We demonstrate here that *A. nidulans* SVs do not have the same requirements as EEs to engage dynein: both fail to engage dynein in p25Δ cells, but SVs, unlike EEs, do not require HookA. The EE specificity of the Hook/FTH complex has been clarified by the finding that a complex

containing Hook1/3 and FHIP behaves as a RAB5 effector (Guo *et al.*, 2016). Of note, the lack of Hook involvement in RabE^{RAB11} SV transport was not predictable a priori. Although the three mammalian Hook paralogues have been associated with endosomes (Xu *et al.*, 2008; Maldonado-Báez *et al.*, 2013), Hook3 reportedly localizes to the Golgi (Walenta *et al.*, 2001), and Hook2 participates in the morphogenesis of the primary cilium (Baron Gaillard *et al.*, 2011), a process that is regulated by a RAB cascade involving the RabE orthologue RAB11 (Das and Guo, 2011; Vetter *et al.*, 2015).

Both SVs and EEs require p25 to engage dynein. Because dynactin lacking p25 or p27 is stable (Zhang *et al.*, 2011b; Yeh *et al.*, 2012), EE and SV trafficking defects seen in p25-null mutant cells appear to reflect a broad role of p25 in cargo recognition rather than dynactin disorganization. This agrees with the contention that p25 is conveniently positioned within the dynein–dynactin structure to mediate direct binding to different cargoes (Yeh *et al.*, 2012). However, rather than directly bridging dynein to membranes, the p25-mediated interaction between dynein–dynactin and *A. nidulans* EEs necessitates HookA (Zhang *et al.*, 2014), predictably recruited to EEs by RAB5s, as demonstrated for neurons (Guo *et al.*, 2016). This suggests that there exists an as-yet-unidentified RabE^{RAB11} effector acting as dynein adaptor, collaborating with p25 in the engagement of SVs, and, potentially, facilitating dynein processivity (McKenney *et al.*, 2014; Olenick *et al.*, 2016; Schroeder and Vale, 2016). Of note, sequence searches could not identify *A. nidulans* homologues of the coiled-coil–containing prototypic mammalian RAB11 effector and dynein adaptor FIP3 (Horgan *et al.*, 2010)

In addition to dynein pathway mutants, ablation of kinesin-1 results in a dynein deficit at the tip (Zhang *et al.*, 2003; Lenz *et al.*, 2006) and impairs the retrograde movement of SVs (this work). Kinesin-mediated dynein localization at the microtubule plus ends is conserved from fungi to neurons (Zhang *et al.*, 2003; Roberts *et al.*, 2014; Twelvetrees *et al.*, 2016). Our data, however, show markedly decreased yet detectable accumulation of dynein in the plus ends of MTs of *kinAΔ* tips, indicating that kinesin-independent mechanisms for dynein's plus-end accumulation, such as direct recruitment from the cytoplasm, may be operative (Zhang *et al.*, 2003; Markus *et al.*, 2011; Cianfrocco *et al.*, 2015). In this regard, dynein might also hitchhike on anterogradely moving RabE^{RAB11} SVs to reach the tip in a myosin-dependent (thus kinesin-1–independent) manner.

As to why dynein engages and subsequently moves SV membranes retrogradely away from their normal destination, we can only speculate. One possibility is that the deposition of septa requires transport of SVs containing cell wall–modifying enzymes. These SVs would move in opposite direction to that required for apical extension. A second is that dynein is involved in a recycling pathway by which some SV membranes return to the TGN. A third possibility accommodates the observations that the relative proportion of retrograde SV movements increases dramatically in *myoEΔ* tips and that dynein transport is uncovered by removing AF transport: dynein engagement ensures that if the interplay between kinesin-1 and myosin-5 fails, SVs may move retrogradely before having a second chance of productively returning to the apex using anterograde motors (Pantazopoulou *et al.*, 2014).

Finally, we point out that this relay model by which transport of RabE^{RAB11} SVs depends on the anterograde (centrifugal) action of kinesin-1 and myosin-5 motors opposing the retrograde (centripetal) action of dynein resembles that proposed for melanophore transport (Wu *et al.*, 1998), although in the latter, it is kinesin-2 rather than kinesin-1 that mediates the plus end–directed MT-dependent step (Levi *et al.*, 2006; Kural *et al.*, 2007).

MATERIALS AND METHODS

Aspergillus techniques and strains

Complete (MCA) and synthetic complete (SC) media (Cove, 1966) containing 1% glucose and 5 mM ammonium tartrate as carbon and nitrogen source, respectively, were routinely employed, with the exception of microscopy cultures (see later description). The complete genotypes of strains used for this work are listed in Supplemental Table S1. The rigor condition of KinA^{G97E} and UncA^{G116E} mutant kinesins was described previously (Zekert and Fischer, 2009). Site-directed mutagenesis of *kinA* and *uncA* was used to generate mutant genes encoding KinA^{G97E} and UncA^{G116E} (the latter S-tagged in the C-terminus). This was followed by gene replacement after transformation with appropriate DNA fragments assembled by fusion PCR (Szewczyk *et al.*, 2006). Transformation used *Aspergillus fumigatus pyrG* (*pyrGAf*) as selective marker. The recipient strain was RQ54 (*pyrG89*; *wA2*; *argB2*::[*argB*-alcAp*::mCherry-*RabA*]; *nkuAΔ*::*argB pyroA4*; Qiu *et al.*, 2013; *nkuAΔ* prevents nonhomologous recombination; Nayak *et al.*, 2005). The resulting *kinA^{G97E}* and *uncA^{G116E}* mutant alleles were verified by DNA sequencing after PCR amplification of the genes from genomic DNA. Deletion alleles of *kinA* (AN5343), *uncA* (AN7547), and *kipA* (AN8286) were made by substituting their complete coding regions by *A. fumigatus pyrG* or *riboB*, as appropriate (Supplemental Table S1).

DNA extraction for PCR genotyping of microcolonies

Entire microcolonies growing from ascospores were dispersed in 100 µl of 10 mM Tris-HCl, pH 8, 2% (vol/vol) Triton X-100, 1% (wt/vol) SDS, 0.1 M NaCl, and 1 mM EDTA and disrupted by incubation at 70°C over a 30-min period with frequent vortexing. Proteins were removed by a single extraction with phenol/chloroform/isoamyl alcohol (25:24:1), and 0.5–1 µl of the recovered aqueous phase was used as DNA template in diagnostic PCRs.

General microscopy techniques and image acquisition

Unless otherwise indicated, epifluorescence microscopy was carried out with hyphae cultured in pH 6.8 watch minimal medium (WMM) at 28°C, using eight-well chambers (IBIDI, Martinsried, Germany, or Lab-Tek, Nalge Nunc International, Rochester, NY) and a Leica DMI6000 B inverted microscope equipped with a Leica 63×/1.4 numerical aperture Plan Apochromatic objective. The temperature of the chamber was controlled with a Heating Insert P on-stage incubator (Leica) and an objective heater (PeCon, Germany), as described (Pinar *et al.*, 2013). Culture temperature in experiments with heat-sensitive mutations was monitored within the wells using a wire thermometer. Cultures reached 37°C within 15–20 min after the shift (Pinar *et al.*, 2013). Latrunculin B was used at a final concentration of 0.1 mM, a concentration previously shown to completely depolymerize F-actin of endocytic patches within 2 min (Pantazopoulou and Peñalva, 2009).

The microscope, driven by MetaMorph Premier software (Molecular Dynamics), was equipped with a Leica EL6000 excitation source, which was set to the minimal intensity compatible with exposure times ranging from 100–250 ms to image the fluorescent proteins used in this work, except in the case of NudA-GFPx3, which required the maximal intensity of the excitation lamp combined with exposure times of up to 600 ms when imaged in *kinAΔ* hyphae. Fluorescence images were captured with a Hamamatsu ORCA ER digital camera (1344 × 1024 pixels) using, for single-channel acquisition, Semrock GFP–3035B and TXRED-4040B BrightLine filter cubes. For simultaneous channel acquisition, we used a Dual-View beam splitter (Photometrics) equipped with the supplier's filter sets for GFP and mCherry fluorescence channels.

To optimize time resolution, movies were acquired using the streaming function of the software, and the smallest possible region of interest was selected to reduce the time needed to discharge the interline charge-coupled device (CCD) light sensor to the computer RAM.

Fluorescent proteins

GFP-RabE^{RAB11} is an N-terminally tagged version of the exocytic RAB expressed under the control of its own promoter (Pantazopoulou *et al.*, 2014). mCherry-RabA^{RAB5} expression was driven by a single-copy integration transgene controlled by the *alcA* (alcohol dehydrogenase) gene promoter. α-Tubulin-GFP (TubA-GFP) was expressed from a single copy of the transgene integrated at the *wA* (white) locus. *myoEΔ* and *wA::tubA-GFP* strains used as parental strains for subsequent crosses were a generous gift of Berl Oakley (University of Kansas, Lawrence, KS). The parental *nudA-GFPx3* strain used to study dynein in the *kinAΔ* background was a generous gift from Samara Reck-Peterson (University of California, San Diego).

To drive mCherry-RabA^{RAB5} expression, we used our single-copy transgene based on the *alcA^p* promoter (Abenza *et al.*, 2009). *alcA^p* is induced by ethanol and repressed by glucose. Overexpression of mCherry-RabA^{RAB5} leads to detection of aggregates of EEs, presumably resulting from homotypic fusion of endosomes promoted by the excessive levels of RAB5. To prevent overexpression, we used D-fructose as C source. This noninduced and nonrepressing sugar result in levels of expression that resemble the physiological levels of RabA^{RAB5} (Abenza *et al.*, 2009). Using a 0.05% (wt/vol) concentration of fructose in overnight cultures, we achieved very homogeneous levels of induction in all hyphae of the population, with very little aggregation of EEs, which markedly facilitated the tracking of EE trajectories with kymographs traced across middle planes of individual hyphae. These kymographs were used to measure the speed of EEs at 28°C using the MetaMorph plug-in.

Image manipulation

All images and time series were processed using different plug-ins of MetaMorph 7.7.0, converted to 8-bit grayscale or 24-bit RGB and annotated with Corel Draw (Corel, Ottawa, Canada). When appropriate, images were corrected with the MetaMorph unsharp mask filter, using a kernel size of 6–9 and a scaling factor of 0.75. Precise alignment of Dual View channels was carried out using the color align menu of MetaMorph and distinctive features in the images as internal references or, when needed, fluorescent beads (TetraSpeck microspheres, blue/green/orange/dark red; Molecular Probes). Single channels are usually shown in inverted grayscale. Annotated movies were converted to QuickTime using ImageJ 1.49s and file sizes adjusted using mpeg-4 compression.

Image and statistical analyses

GraphPad Prism 3.02 (GraphPad Software) was used for statistical analysis and graphical displays of data sets. SigmaPlot 11.0 (Systat Software) was used to plot line scans with data obtained by the MetaMorph line scan plug-in.

To determine the speed of SVs in wt or *hookAΔ* cells treated with latB, we used time series acquired for middle planes of hyphal tip cells. These time stacks were used to draw 20-µm-long kymographs with segmented lines starting at the apex. Trajectories of moving vesicles were tracked manually on these kymographs. The tracks were used to classify runs into anterograde and retrograde classes and calculate individual speeds using the MetaMorph kymograph plug-in. The mean speeds of anterograde and retrograde runs were significantly different at 28 and 37°C using two-tailed unpaired *t* testing with Welch's correction (see the legends to Figures 1 and 2). The speed of EEs in the wt (Figure 6C) was determined with kymographs of mCherry-RabA^{RAB5}, similarly to SVs (we observed nearly complete or complete absence of EE runs in *hookAΔ*, *p25Δ*, *kinA^{G97E}*, and *uncA^{G116E}* hyphae).

Apical extension rates (Figure 5D) were calculated from time-lapse series of hyphae growing on the stage in microscopy chambers containing WMM with 0.1% glucose as C source. Images were acquired with the Nomarski optics at 6–12 frames/min over at least 20 min. The resulting time series were used to draw kymographs across the growing tips. In these plots, a growing tip showed up as a diagonal line traced by the extending apex, the slope of which was used to deduce actual apical extension rates (with the MetaMorph kymograph plug-in). Growth rates are exquisitely dependent on the incubation temperature. To optimize growth, we inoculated culture chambers that were incubated overnight at 26°C. These chambers were then transferred to the microscopy room, which had been adjusted to 28–29°C. Upon placement of the culture chamber onto the prewarmed microscope, the objective heater and the stage incubator were set at 29 and 28°C, respectively, and cultures were allowed to grow for a further 60–90 min before acquisition of time series. Under these controlled conditions, the temperature of the medium during image acquisition was 29 ± 0.5°C.

To provide a quantitative estimation of the accumulation of GFP-RabE^{RAB11} SVs in the SPK (Figure 5E), we measured the fluorescence intensity of sum projections of *z*-stacks (11 planes; *z* pass, 0.25 µm) in a circular region of interest (24 pixels, ~4.5 µm^2) encompassing the totality of the SPK (subtracting the background determined in an empty equivalent region). Data sets were compared by one-way analysis-of-variance (ANOVA), followed by Bonferroni's multiple comparison test. Data sets were represented as scatter plots with means and, unless otherwise indicated in the figure legends, 95% confidence interval (CI) bars.

To estimate the flux of SVs circulating on the MTs across the apicalmost 20 µm of wt and mutant cells treated with latB (Figures 3C and 8C), we used kymographs derived from lines that started at the apex and counted manually, using MetaMorph, the number of runs per time unit in each direction in a sample of cells. The resulting data sets, which passed the Kolmogorov–Smirnov normality test, were compared by one-way ANOVA followed by Bonferroni's multiple comparison test.

The fact that EE runs were less numerous and that the fluorescence was more homogeneous compared with SVs in latB-treated cells facilitated the tracking of the total distance covered by EE runs per unit time in either direction in a sample of five hyphae (Figure 6D; for calculations, 20-µm kymographs were plotted from mCherry-RabA^{RAB5} time series). Data sets were compared by one-way ANOVA followed by Bonferroni's multiple comparison test.

To obtain an approximate estimation of the flux of SVs attributable to MT transport in untreated wt, *kinA^{G97E}*, and *uncA^{G116E}* hyphae (Figure 7D), we used GFP-RabE^{RAB11} time series to plot kymographs. Rather than starting at the apex, the 10-µm-long segments that we used for these kymographs excluded the 2- to 4-µm apicalmost region, seeking to analyze flux across slightly subapical regions where AF transport is expected to be less active (although not absent, as some AFs can very likely extend beyond the excluded region). This design also facilitated visualization of the faint runs that we attribute to MT transport, as the strongly fluorescence SPK was excluded. Kymographs were used to count manually the total number of anterograde and retrograde runs. Data sets were analyzed by one-way ANOVA followed by Bonferroni's multiple comparison test.

Kymographs of NudA-GFP were used to estimate with MetaMorph the MT growth in wt cells (Figure 4C). To acquire time series of NudA-GFP in *kinAΔ* cells, we used the maximal excitation power of a Leica EL6000 external light source with metal halide lamp for epifluorescence excitation, 400- to 600-ms exposure times, and the maximal gain setting of the an ORCA-ER II CCD camera.

ACKNOWLEDGMENTS

We thank Reinhard Fisher and Natalia Requena for the *kinA::pyr-4* disruption allele, Berl Oakley for *myoEΔ*, *tubA-GFP,* and *myoE-GFP* alleles, Samara Reck-Peterson for the gene-replaced *nudA-3xGFP* strain, Elena Reoyo for technical assistance, and four anonymous referees for suggesting valuable improvements to the first version of the manuscript. This work was funded by grants from the Spanish Ministerio de Economía y Competitividad (BIO2012-30965 and BIO2015-65090-R) and the Comunidad de Madrid (Grant S2010/BMD-2414) to M.A.P. and from the National Institutes of Health (RO1 GM097580) and the Uniformed Services University (intramural grant BIO-71-1972) to X.X.

REFERENCES

Abenza JF, Galindo A, Pantazopoulou A, Gil C, de los Ríos V, Peñalva MA (2010). *Aspergillus* RabB^{Rab5} integrates acquisition of degradative identity with the long-distance movement of early endosomes. Mol Biol Cell 21, 2756–2769.

Abenza JF, Galindo A, Pinar M, Pantazopoulou A, de los Ríos V, Peñalva MA (2012). Endosomal maturation by Rab conversion in *Aspergillus nidulans* is coupled to dynein-mediated basipetal movement. Mol Biol Cell 23, 1889–1901.

Abenza JF, Pantazopoulou A, Rodríguez JM, Galindo A, Peñalva MA (2009). Long-distance movement of *Aspergillus nidulans* early endosomes on microtubule tracks. Traffic 10, 57–75.

Akhmanova A, Hammer JA III (2010). Linking molecular motors to membrane cargo. Curr Opin Cell Biol 22, 479–487.

Baron Gaillard CL, Pallesi-Pocachard E, Massey-Harroche D, Richard F, Arsanto JP, Chauvin JP, Lecine P, Krämer H, Borg JP, Le Bivic A (2011). Hook2 is involved in the morphogenesis of the primary cilium. Mol Biol Cell 22, 4549–4562.

Bielska E, Schuster M, Roger Y, Berepiki A, Soanes DM, Talbot NJ, Steinberg G (2014). Hook is an adapter that coordinates kinesin-3 and dynein cargo attachment on early endosomes. J Cell Biol 204, 989–1007.

Carter AP, Diamant AG, Urnavicius L (2016). How dynein and dynactin transport cargos: a structural perspective. Curr Opin Struct Biol 37, 62–70.

Chesarone-Cataldo M, Guérin C, Yu, Jerry H, Wedlich-Soldner R, Blanchoin L, Goode, Bruce L (2011). The myosin passenger protein Smy1 controls actin cable structure and dynamics by acting as a formin damper. Dev Cell 21, 217–230.

Chowdhury S, Ketcham SA, Schroer TA, Lander GC (2015). Structural organization of the dynein-dynactin complex bound to microtubules. Nat Struct Mol Biol 22, 345–347.

Cianfrocco MA, DeSantis ME, Leschziner AE, Reck-Peterson SL (2015). Mechanism and regulation of cytoplasmic dynein. Annu Rev Cell Dev Biol 31, 83–108.

Cove DJ (1966). The induction and repression of nitrate reductase in the fungus *Aspergillus nidulans*. Biochim Biophys Acta 113, 51–56.

Das A, Guo W (2011). Rabs and the exocyst in ciliogenesis, tubulogenesis and beyond. Trends Cell Biol 21, 383–386.

Eckley DM, Gill SR, Melkonian KA, Bingham JB, Goodson HV, Heuser JE, Schroer TA (1999). Analysis of dynactin subcomplexes reveals a novel actin-related protein associated with the Arp1 minifilament pointed end. J Cell Biol 147, 307–320.

Egan MJ, Tan K, Reck-Peterson SL (2012). Lis1 is an initiation factor for dynein-driven organelle transport. J Cell Biol 197, 971–982.

Fu M-M, Holzbaur ELF (2014). Integrated regulation of motor-driven organelle transport by scaffolding proteins. Trends Cell Biol 24, 564–574.

Guimaraes SC, Schuster M, Bielska E, Dagdas G, Kilaru S, Meadows BR, Schrader M, Steinberg G (2015). Peroxisomes, lipid droplets, and endoplasmic reticulum "hitchhike" on motile early endosomes. J Cell Biol 211, 945–954.

Guo X, Farías GG, Mattera R, Bonifacino JS (2016). Rab5 and its effector FHF contribute to neuronal polarity through dynein-dependent retrieval of somatodendritic proteins from the axon. Proc Natl Acad Sci USA 113, E5318–E5327.

Haag C, Steuten B, Feldbrügge M (2015). Membrane-coupled mRNA trafficking in fungi. Annu Rev Microbiol 69, 265–281.

Hammer JA 3rd, Sellers JR (2012). Walking to work: roles for class V myosins as cargo transporters. Nat Rev Mol Cell Biol 13, 13–26.

Han G, Liu B, Zhang J, Zuo W, Morris NR, Xiang X (2001). The Aspergillus cytoplasmic dynein heavy chain and NUDF localize to microtubule ends and affect microtubule dynamics. Curr Biol 11, 719–724.

Higuchi Y, Ashwin P, Roger Y, Steinberg G (2014). Early endosome motility spatially organizes polysome distribution. J Cell Biol 204, 343–357.

Hodges AR, Bookwalter CS, Krementsova EB, Trybus KM (2009). A nonprocessive class V myosin drives cargo processively when a kinesin-related protein is a passenger. Curr Biol 19, 2121–2125.

Hoogenraad CC, Akhmanova A, Howell SA, Dortland BR, De Zeeuw CI, Willemsen R, Visser P, Grosveld F, Galjart N (2001). Mammalian Golgi-associated Bicaudal-D2 functions in the dynein–dynactin pathway by interacting with these complexes. EMBO J 20, 4041–4054.

Horgan CP, Hanscom SR, Jolly RS, Futter CE, McCaffrey MW (2010). Rab11-FIP3 links the Rab11 GTPase and cytoplasmic dynein to mediate transport to the endosomal-recycling compartment. J Cell Sci 123, 181–191.

Horio T, Oakley BR (2005). The role of microtubules in rapid hyphal tip growth of *Aspergillus nidulans*. Mol Biol Cell 16, 918–926.

Huang J, Roberts AJ, Leschziner AE, Reck-Peterson SL (2012). Lis1 acts as a "clutch" between the ATPase and microtubule-binding domains of the dynein motor. Cell 150, 975–986.

Huang J-D, Brady ST, Richards BW, Stenoien D, Resau JH, Copeland NG, Jenkins NA (1999). Direct interaction of microtubule- and actin-based transport motors. Nature 397, 267–270.

Johansson M, Rocha N, Zwart W, Jordens I, Janssen L, Kuijl C, Olkkonen VM, Neefjes J (2007). Activation of endosomal dynein motors by stepwise assembly of Rab7–RILP–p150Glued, ORP1L, the receptor βIII spectrin. J Cell Biol 176, 459–471.

Konzack S, Rischitor PE, Enke C, Fischer R (2005). The role of the kinesin motor KipA in microtubule organization and polarized growth of *Aspergillus nidulans*. Mol Biol Cell 16, 497–506.

Kural C, Serpinskaya AS, Chou Y-H, Goldman RD, Gelfand VI, Selvin PR (2007). Tracking melanosomes inside a cell to study molecular motors and their interaction. Proc Natl Acad Sci USA 104, 5378–5382.

Lenz JH, Schuchardt I, Straube A, Steinberg G (2006). A dynein loading zone for retrograde endosome motility at microtubule plus-ends. EMBO J 25, 2275–2286.

Levi V, Serpinskaya AS, Gratton E, Gelfand V (2006). Organelle transport along microtubules in xenopus melanophores: Evidence for cooperation between multiple motors. Biophys J 90, 318–327.

Lwin KM, Li D, Bretscher A (2016). Kinesin-related Smy1 enhances the Rab-dependent association of myosin-V with secretory cargo. Mol Biol Cell 27, 2450–2462.

Maldonado-Báez L, Cole NB, Krämer H, Donaldson JG (2013). Microtubule-dependent endosomal sorting of clathrin-independent cargo by Hook1. J Cell Biol 201, 233–247.

Markus SM, Plevock KM, St Germain BJ, Punch JJ, Meaden CW, Lee WL (2011). Quantitative analysis of Pac1/LIS1-mediated dynein targeting: Implications for regulation of dynein activity in budding yeast. Cytoskeleton (Hoboken) 68, 157–174.

McKenney RJ, Huynh W, Tanenbaum ME, Bhabha G, Vale RD (2014). Activation of cytoplasmic dynein motility by dynactin-cargo adapter complexes. Science 345, 337–341.

Nayak T, Szewczyk E, Oakley CE, Osmani A, Ukil L, Murray SL, Hynes MJ, Osmani SA, Oakley BR (2005). A versatile and efficient gene targeting system for *Aspergillus nidulans*. Genetics 172, 1557–1566.

Olenick MA, Tokito M, Boczkowska M, Dominguez R, Holzbaur ELF (2016). Hook adaptors induce unidirectional processive motility by enhancing the dynein-dynactin interaction. J Biol Chem 291, 18239–18251.

Pantazopoulou A, Peñalva MA (2009). Organization and dynamics of the *Aspergillus nidulans* Golgi during apical extension and mitosis. Mol Biol Cell 20, 4335–4347.

Pantazopoulou A, Pinar M, Xiang X, Peñalva MA (2014). Maturation of late Golgi cisternae into RabE^{RAB11} exocytic post-Golgi carriers visualized *in vivo*. Mol Biol Cell 25, 2428–2443.

Peñalva MA, Galindo A, Abenza JF, Pinar M, Calcagno-Pizarelli AM, Arst HN Jr, Pantazopoulou A (2012). Searching for gold beyond mitosis: mining intracellular membrane traffic in *Aspergillus nidulans*. Cell Logist 2, 2–14.

Pinar M, Arst HN Jr, Pantazopoulou A, Tagua VG, de los Ríos V, Rodríguez-Salarichs J, Díaz JF, Peñalva MA (2015). TRAPPII regulates exocytic Golgi exit by mediating nucleotide exchange on the Ypt31 orthologue RabE/RAB11. Proc Natl Acad Sci USA 112, 4346–4351.
Pinar M, Pantazopoulou A, Arst HN Jr, Peñalva MA (2013). Acute inactivation of the *Aspergillus nidulans* Golgi membrane fusion machinery: correlation of apical extension arrest and tip swelling with cisternal disorganization. Mol Microbiol 89, 228–248.
Pohlmann T, Baumann S, Haag C, Albrecht M, Feldbrügge M (2015). A FYVE zinc finger domain protein specifically links mRNA transport to endosome trafficking. Elife 4, e06041.
Qiu R, Zhang J, Xiang X (2013). Identification of a novel site in the tail of dynein heavy chain important for dynein function in vivo. J Biol Chem 288, 2271–2280.
Reck-Peterson SL, Provance DW Jr, Mooseker MS, Mercer JA (2000). Class V myosins. Biochim Biophys Acta 1496, 36–51.
Requena N, Alberti-Segui C, Winzenburg E, Horn C, Schliwa M, Philippsen P, Liese R, Fischer R (2001). Genetic evidence for a microtubule-destabilizing effect of conventional kinesin and analysis of its consequences for the control of nuclear distribution in *Aspergillus nidulans*. Mol Microbiol 42, 121–132.
Roberts AJ, Goodman BS, Reck-Peterson SL (2014). Reconstitution of dynein transport to the microtubule plus end by kinesin. Elife 3, e02641.
Salogiannis J, Egan MJ, Reck-Peterson SL (2016). Peroxisomes move by hitchhiking on early endosomes using the novel linker protein PxdA. J Cell Biol 212, 289–296.
Salogiannis J, Reck-Peterson SL (2017). Hitchhiking: a non-canonical mode of microtubule-based transport. Trends Cell Biol 27, 141–150.
Scherer J, Yi J, Vallee RB (2014). PKA-dependent dynein switching from lysosomes to adenovirus: a novel form of host–virus competition. J Cell Biol 205, 163–177.
Schmidt H, Zalyte R, Urnavicius L, Carter AP (2015). Structure of human cytoplasmic dynein-2 primed for its power stroke. Nature 518, 435–438.
Schroeder CM, Vale RD (2016). Assembly and activation of dynein–dynactin by the cargo adaptor protein Hook3. J Cell Biol 214, 309–318.
Schroeder HW III, Mitchell C, Shuman H, Holzbaur ELF, Goldman YE (2010). Motor number controls cargo switching at actin-microtubule intersections in vitro. Curr Biol 20, 687–696.
Schuster M, Lipowsky R, Assmann MA, Lenz P, Steinberg G (2011). Transient binding of dynein controls bidirectional long-range motility of early endosomes. Proc Natl Acad Sci USA 108, 3618–3623.
Schuster M, Martin-Urdiroz M, Higuchi Y, Hacker C, Kilaru S, Gurr SJ, Steinberg G (2016). Co-delivery of cell-wall-forming enzymes in the same vesicle for coordinated fungal cell wall formation. Nat Microbiol 1, 16149.
Seidel C, Moreno-Velasquez SD, Riquelme M, Fischer R (2013). *Neurospora crassa* NKIN2, a kinesin-3 motor, transports early endosomes and is required for polarized growth. Eukaryot Cell 12, 1020–1032.
Seidel C, Zekert N, Fischer R (2012). The Aspergillus nidulans kinesin-3 tail Is necessary and sufficient to recognize modified microtubules. PLoS One 7, e30976.
Sharpless KE, Harris SD (2002). Functional characterization and localization of the *Aspergillus nidulans* formin SEPA. Mol Biol Cell 13, 469–479.
Steinberg G (2014). Endocytosis and early endosome motility in filamentous fungi. Curr Opin Microbiol 20, 10–18.
Straube A, Hause G, Fink G, Steinberg G (2006). Conventional kinesin mediates microtubule-microtubule interactions in vivo. Mol Biol Cell 17, 907–916.
Szewczyk E, Nayak T, Oakley CE, Edgerton H, Xiong Y, Taheri-Talesh N, Osmani SA, Oakley BR (2006). Fusion PCR and gene targeting in Aspergillus nidulans. Nat Protoc 1, 3111–3120.
Taheri-Talesh N, Horio T, Araujo-Bazán L, Dou X, Espeso EA, Peñalva MA, Osmani SA, Oakley BR (2008). The tip growth apparatus of *Aspergillus nidulans*. Mol Biol Cell 19, 1439–1449.
Taheri-Talesh N, Xiong Y, Oakley BR (2012). The functions of myosin II and myosin V homologs in tip growth and septation in *Aspergillus nidulans*. PLoS One 7, e31218.
Takeshita N, Wernet V, Tsuizaki M, Grun N, Hoshi HO, Ohta A, Fischer R, Horiuchi H (2015). Transportation of aspergillus nidulans Class III and V chitin synthases to the hyphal tips depends on conventional kinesin. PLoS One 10, e0125937.
Toropova K, Zou S, Roberts AJ, Redwine WB, Goodman BS, Reck-Peterson SL, Leschziner AE (2014). Lis1 regulates dynein by sterically blocking its mechanochemical cycle. Elife 3, 10.7554/eLife.03372.
Twelvetrees AE, Pernigo S, Sanger A, Guedes-Dias P, Schiavo G, Steiner RA, Dodding MP, Holzbaur ELF (2016). The dynamic localization of cytoplasmic dynein in neurons is driven by kinesin-1. Neuron 90, 1000–1015.
Urnavicius L, Zhang K, Diamant AG, Motz C, Schlager MA, Yu M, Patel NA, Robinson CV, Carter AP (2015). The structure of the dynactin complex and its interaction with dynein. Science 347, 1441–1446.
Vale RD (2003). The molecular motor toolbox for intracellular transport. Cell 112, 467–480.
Vetter M, Stehle R, Basquin C, Lorentzen E (2015). Structure of Rab11-FIP3-Rabin8 reveals simultaneous binding of FIP3 and Rabin8 effectors to Rab11. Nat Struct Mol Biol 22, 695–702.
Walenta JH, Didier AJ, Liu X, Krämer H (2001). The Golgi-associated Hook3 protein is a member of a novel family of microtubule-binding proteins. J Cell Biol 152, 923–934.
Wedlich-Soldner R, Straube A, Friedrich MW, Steinberg G (2002). A balance of KIF1A-like kinesin and dynein organizes early endosomes in the fungus *Ustilago maydis*. EMBO J 21, 2946–2957.
Wu X, Bowers B, Rao K, Wei Q, Hammer JA 3rd (1998). Visualization of melanosome dynamics within wild-type and dilute melanocytes suggests a paradigm for myosin V function In vivo. J Cell Biol 143, 1899–1918.
Xiang X, Han G, Winkelmann DA, Zuo W, Morris NR (2000). Dynamics of cytoplasmic dynein in living cells and the effect of a mutation in the dynactin complex actin-related protein Arp1. Curr Biol 10, 603–606.
Xiang X, Qiu R, Yao X, Arst HN Jr, Peñalva MA, Zhang J (2015). Cytoplasmic dynein and early endosome transport. Cell Mol Life Sci 72, 3267–3280.
Xu L, Sowa ME, Chen J, Li X, Gygi SP, Harper JW (2008). An FTS/Hook/p107(FHIP) complex interacts with and promotes endosomal clustering by the homotypic vacuolar protein sorting complex. Mol Biol Cell 19, 5059–5071.
Yao X, Arst HN, Wang X, Xiang X (2015). Discovery of a vezatin-like protein for dynein-mediated early endosome transport. Mol Biol Cell 26, 3816–3827.
Yao X, Wang X, Xiang X (2014). FHIP and FTS proteins are critical for dynein-mediated transport of early endosomes in Aspergillus. Mol Biol Cell 25, 2181–2189.
Yeh T-Y, Quintyne NJ, Scipioni BR, Eckley DM, Schroer TA (2012). Dynactin's pointed-end complex is a cargo-targeting module. Mol Biol Cell 23, 3827–3837.
Zander S, Baumann S, Weidtkamp-Peters S, Feldbrügge M (2016). Endosomal assembly and transport of heteromeric septin complexes promote septin cytoskeleton formation. J Cell Sci 129, 2778–2792.
Zekert N, Fischer R (2009). The *Aspergillus nidulans* kinesin-3 UncA motor moves vesicles along a subpopulation of microtubules. Mol Biol Cell 20, 673–684.
Zhang J, Li S, Fischer R, Xiang X (2003). Accumulation of cytoplasmic dynein and dynactin at microtubule plus ends in *Aspergillus nidulans* is kinesin dependent. Mol Biol Cell 14, 1479–1488.
Zhang J, Qiu R, Arst HN Jr, Penalva MA, Xiang X (2014). HookA is a novel dynein-early endosome linker critical for cargo movement in vivo. J Cell Biol 204, 1009–1026.
Zhang J., Tan K, Wu X, Chen G, Sun J, Reck-Peterson SL, Hammer JA 3rd, Xiang X (2011a). *Aspergillus* Myosin-v supports polarized growth in the absence of microtubule-based transport. PLoS One 6, e28575.
Zhang J, Yao X, Fischer L, Abenza JF, Penalva MA, Xiang X (2011b). The p25 subunit of the dynactin complex is required for dynein-early endosome interaction. J Cell Biol 193, 1245–1255.
Zhang J, Zhuang L, Lee Y, Abenza JF, Peñalva MA, Xiang X (2010). The microtubule plus-end localization of *Aspergillus* dynein is important for dynein-early-endosome interaction but not for dynein ATPase activation. J Cell Sci 123, 3596–3604.